scientific reports

Check for updates

OPEN

Multiomics reveals metformin's dual role in gut microbiome remodeling and hepatic metabolic reprogramming for MAFLD intervention

Yuan-dong Sun[1,2]✉, Hao Zhang[3], Xiao-long Gong[4], Yuan-min Li[5], Ruiqin Han[6], Chun-xiao Zhou[7] & Jian-jun Han[3]✉

Metabolic Associated Fatty Liver Disease (MAFLD), previously known as Non-Alcoholic Fatty Liver Disease, is a growing global health issue associated with obesity, type 2 diabetes, and metabolic syndrome. This study investigates the potential of metformin, a common anti-diabetic drug, to slow the progression of MAFLD using a multi-omics approach. Male Wistar rats were fed a choline-deficient diet to induce MAFLD and treated with metformin through their drinking water for 48 weeks. We conducted a comprehensive analysis including liver histology, untargeted metabolomics, lipidomics, and gut microbiome profiling to assess the effects of metformin on liver and gut metabolic patterns. Metformin administration led to significant changes in gut microbiome diversity and the abundance of specific microbial species in MAFLD rats. Histological analysis showed that metformin-treated rats had reduced lipid accumulation and fibrosis in the liver compared to untreated MAFLD rats. Metabolomic and lipidomic analyses revealed that metformin corrected abnormal lipid metabolism patterns, reduced hepatic fat deposition, and influenced key metabolic pathways associated with MAFLD progression. Our findings suggest that metformin has a protective role against MAFLD by modulating gut microbiota and liver metabolism, thereby slowing the progression of hepatic fibrosis. This study provides insights into the therapeutic potential of metformin for MAFLD by addressing metabolic pattern disorders and abnormal changes in gut microbial diversity, highlighting its impact on lipid metabolism and gut-liver axis interactions.

Keywords Metabolic associated fatty liver disease, Liver cirrhosis, Metformin, Multi-omics, Liver metabolism

Metabolic Associated Fatty Liver Disease (MAFLD), also known as Metabolic associated fatty liver disease and formerly referred to as Non-Alcoholic Fatty Liver Disease (NAFLD), has emerged as a major non-communicable liver disease globally[1,2]. The escalating prevalence of conditions like obesity, type 2 diabetes, and metabolic syndrome has seen a concurrent surge in MAFLD cases, positioning it as a paramount public health concern[3,4]. Epidemiologically, MAFLD afflicts approximately 25% of the worldwide population, with notable regional disparities. The Middle East and South America report the highest incidences, followed closely by Asia, North America, and Europe[5,6]. The swift urbanization and adoption of unhealthy dietary habits in developing nations have notably amplified the number of MAFLD cases[7,8].

[1]Xinjiang Medical University Affiliated Cancer Hospital, Urumqi, China. [2]Xinjiang Key Laboratory of Translational Biomedical Engineering, Urumqi, China. [3]Department of Interventional Radiology, Shandong Cancer Hospital and Institute Affiliated Shandong First Medical University and Shandong Academy of Medical Sciences, No. 440, Jiyan Road, Ji'nan 250117, Shandong, China. [4]Graduate School of Shandong First Medical University, Ji'nan, China. [5]Key Laboratory of Transplant Engineering and Immunology, NHC, Frontiers Science Center for Disease-Related Molecular Network, West China Hospital, Sichuan University, Cheng'du, China. [6]Department of Biochemistry and Molecular Biology, Institute of Basic Medical Sciences, Chinese Academy of Medical Sciences and Peking Union Medical College, Beijing, China. [7]Division of Gynecologic Oncology, University of North Carolina at Chapel Hill, Chapel, USA. ✉email: 13176829692@163.com; jieruheweichuang@163.com; hanjianjun@sdfmu.edu.cn

Several intertwined risk factors play pivotal roles in MAFLD onset and progression. Central obesity, marked by increased visceral fat, stands out as a primary risk determinant[9,10]. Insulin resistance, frequently resulting from obesity, plays a crucial role in the accumulation of fat in the liver[11]. Chronic liver fibrosis, a consequence of MAFLD, significantly elevates the risk of liver function deterioration in affected individuals[1,12,13]. Genetic predispositions, such as polymorphisms in the PNPLA3 and TM6SF2 genes, heighten MAFLD susceptibility[14]. Importantly, changes in metabolic patterns, notably in lipid and carbohydrate metabolism, critically influence the progression of MAFLD[15–17]. These metabolic alterations can exacerbate hepatic steatosis, inflammation, and fibrosis, accelerating the disease's progression. Understanding and targeting these metabolic shifts is therefore crucial in managing MAFLD. Additionally, gut microbiota imbalances, signified by a disproportionate ratio of beneficial to harmful bacterial species, have been implicated in MAFLD's pathogenesis, though the precise mechanisms remain under exploration[18]. Lean MAFLD patients, despite having a normal or lean body type, face significant risks of liver fat accumulation and fibrosis. Unlike obese MAFLD, the pathogenesis in lean patients is more complex, potentially involving genetic factors, insulin resistance, and gut microbiota imbalances. These patients often find it difficult to improve their condition through standard weight management strategies, making treatment particularly challenging. In summation, the rising tide of MAFLD underscores the urgency for early detection and intervention. Recognizing and addressing these high-risk determinants can pave the way for tailored therapeutic and preventive strategies. As our comprehension of MAFLD deepens, a comprehensive approach encompassing lifestyle modifications, pharmacological interventions, and potential microbiota modulation becomes indispensable in confronting this global health challenge.

Primarily used for treating type 2 diabetes, Metformin lowers blood sugar levels by inhibiting glucose production in the liver and enhancing glucose utilization in muscles[19,20]. Its benefits extend to improving pancreatic β-cell function and increasing insulin sensitivity, reducing insulin resistance[21,22]. The drug's effectiveness in mitigating hepatic fat accumulation has recently positioned it as a key treatment option for metabolic diseases like MAFLD and Metabolic Associated Steatohepatitis[23,24]. Additionally, Metformin's potential in anti-aging, due to its activation of AMP-activated protein kinase (AMPK), a crucial enzyme in energy regulation, by mimicking a state of starvation, is garnering interest[25,26]. Its role in metabolic disease and weight loss research continues to expand, promising new therapeutic discoveries.

To investigate the mechanism by which metformin affects the local hepatic metabolism of diet-induced MAFLD, we utilized Wistar rats that had been fed a choline-deficient diet since weaning as our experimental subjects[27,28]. Long-term intervention was carried out by adding metformin to their drinking water. We observed that lean MAFLD rats shown a significant impact on hepatic metabolic patterns, especially lipid metabolism. Furthermore, we found that in lean MAFLD rats, metformin treatment led to notable differences in gut microbiome composition, metabolic pattern changes, and lipid metabolism. These findings suggest that metformin not only alters hepatic metabolism but also significantly affects the gut microbiota and systemic metabolic processes, contributing to its therapeutic effects in MAFLD.

In summary, our findings bolster a potential notion that during the progression of lean MAFLD liver fibrosis, the use of metformin can modulate hepatic metabolic patterns, leading to some beneficial alterations. While these changes did not significantly improve fat deposition, they did demonstrate a decelerating effect on the progression of fibrosis. Against the backdrop of challenging dietary habits, an increased moderate intake of metformin might offer some health benefits in mitigating lean MAFLD-associated liver fibrosis. Material and methods. Whole workflow is described in Fig. 1A.

Materials and methods

Accordance and approval statement

Our study adhered to all relevant ethical regulations and followed the research protocol approved by the Research Center Ethics Committee of Shandong cancer hospital (SDTHEC2020004088). We confirm that all methods were carried out in accordance with relevant guidelines and regulations. We confirm that all methods are reported in accordance with ARRIVE guidelines (https://arriveguidelines.org). 16 S rRNA sequencing and metabolic analysis were carried out by Lianchuan Biotechnology Co. Ltd (Hangzhou, China).

Portions of the language in this article have been refined and optimized with the assistance of the GPT 4.0 model. The purpose of utilizing the GPT 4.0 model is to enhance the fluency and readability of the text, and not for generating scientific content or data. All scientific viewpoints, data analyses, and conclusions in this study were independently formulated by the authors, without intervention from artificial intelligence tools. We declare this to ensure academic integrity and transparency in our research.

Subject

Our study exclusively examined male rat because male animals exhibited less variability in phenotype. All animal models used in this study were male Wistar rats. The rats were first-generation offspring from a breeding study where the parents had been obtained from HuaFukang Experimental Animal Center (Beijing, China). All rats were born no more than 3 days apart and were weaned on postnatal day 21. All rats were raised in the same standard environment. Each rat cage was housed with only one Wistar rats and they were kept in a light (12-hour light and dark cycle) barrier environment at 22 °C. During this study time, all rats were free to drink water and diet. A total of 25 rats were divided into three subgroups: the blank control group (Control group), the MAFLD-related liver fibrosis group (CDD group), and the metformin intervention group (MI group). The rats in control group were freely accessed to clean water and standard rat diet (Keaoxieli Co. Ltd. Beijing, China). In separate diet-induced MAFLD model in CDD group and MI group, rats were maintained on Choline-Deficient, Amino acid-defined HFD (45 kcal% fat) containing 0.1% methionine (CDAHFD, A06071309, Research Diets Inc. New Brunswick, NJ) for 48 weeks. In contrast to the clean drinking water provided to the CDD group, rats in the MI group had metformin hydrochloride added to their drinking water. The drug was administered to rats

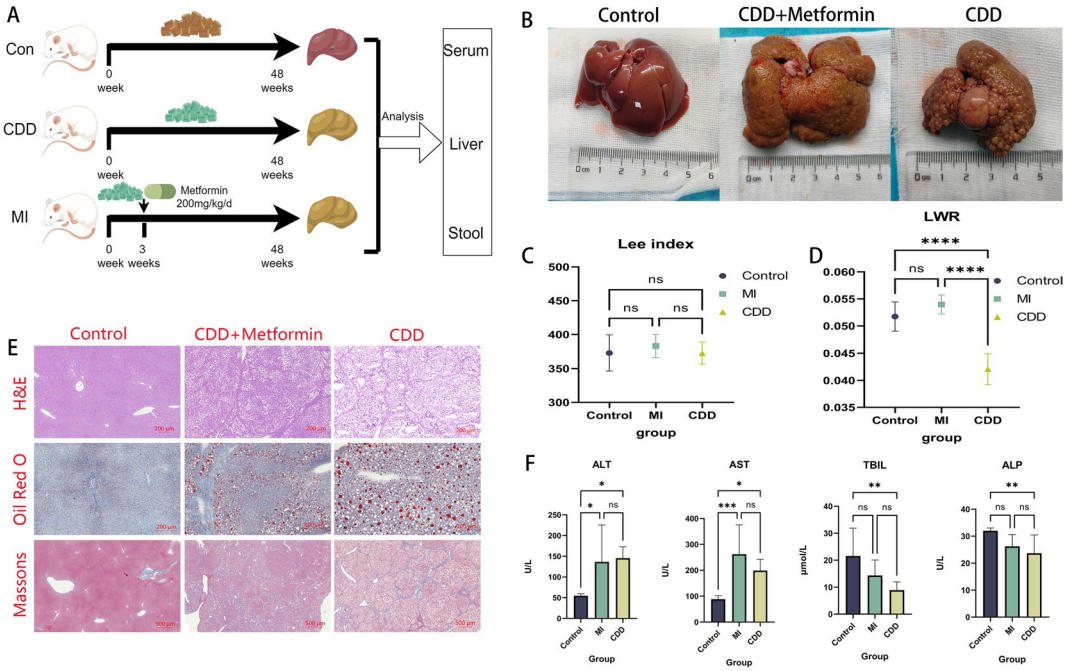

Fig. 1. Metformin treatment improves fat deposition and liver fibrosis in MAFLD. (**A**) Experimental procedure; (**B**) General liver morphology in different rat groups; (**C**) Lee's index in rats; (**D**) LWR in rats; (**E**) H&E, Oil Red O, and Masson's Trichrome staining of rat liver; (**F**) Liver function in rats. Con/Control: control group with standard diet; CDD: choline-deficient high-fat diet group; MI: metformin-treated plus choline-deficient high-fat diet group; LWR: Liver Weight Ratio; p-values obtained via two-tailed unpaired Student's t-tests; $^{*}p<0.05$; $^{**}p<0.01$; $^{***}p<0.001$; $^{****}p<0.0001$; ns: no significance.

by dissolving metformin (Aladdin Inc., Shanghai, China) in water, and the drug concentration was adjusted according to changes in the amount of water consumed by the rats to ensure that the daily dose of the drug ingested was approximately 200 mg/kg/d. The metformin intervention started concurrently with the CDD diet and lasted for 48 weeks.

Rats were anesthetized using inhalational anesthesia with a small animal anesthesia machine (RWD Inc., Shenzhen, China), inducing anesthesia with 3% isoflurane followed by maintenance at 1.5% isoflurane. Then we measured body weight and length to calculate Lee's index (Lee's index = body weight^3 /body length*100), and weighed the liver to calculate the ratio of liver to body weight. Blood samples were obtained via cardiac puncture, and serum samples were extracted by centrifugation (3500 rpm, $r = 10$ cm, 10 min), then stored at -80℃ until analysis. Hematology analysis of blood samples was performed using an auto hematology analyzer BC-2600 vet (Mindray Biomedical Electronics Co., Ltd., Shenzhen, China) following the manufacturer's instructions. After blood collection, the liver and kidneys were excised and weighed. The levels of AST and ALT in both blood samples and liver tissues were determined using an automated Chemray-240 clinical analyzer (Rayto Co., Ltd., Shenzhen, China).

In this experiment, the hematological analysis of rat blood samples was conducted using the Mindray BC-5000vet fully automated hematology analyzer. Samples were prepared following the manufacturer's guidelines to ensure quality control throughout the collection and processing of the rat blood specimens. The analyzer automatically performed the counting and classification of blood cells, including red blood cells (RBCs), white blood cells (WBCs), and platelets (PLTs). It also provided detailed parameters such as red cell distribution width (RDW), mean corpuscular volume (MCV), and the neutrophil to lymphocyte ratio (NLR). The index of neutrophil to lymphocyte ratio is calculated by dividing the count of neutrophils by the count of lymphocytes. This ratio is derived from a standard Complete Blood Count (CBC). The formula is: NLR = Lymphocyte count/Neutrophil count..

The quantification of hepatic lipid accumulation was conducted by randomly selecting three non-overlapping fields of view from Oil Red O-stained liver specimens of four rats each from the CDD and MI groups (A total of 12 images) by ImageJ software (National Institutes of Health, US). The proportion of the area occupied by red lipid droplets was calculated to quantify the accumulation of lipids.

In research protocols, rats were euthanized under strict ethical guidelines. After inducing deep anesthesia using isoflurane inhalation via a gas anesthesia chamber, blood samples were collected via terminal cardiac puncture. To ensure sustained unconsciousness during the procedure, an anesthetic facemask maintained continuous isoflurane delivery. Following blood collection, cervical dislocation was performed as the secondary euthanasia method while the animal remained fully anesthetized, minimizing distress. Death was confirmed by absence of reflexes and cardiopulmonary arrest. This dual-phase approach complies with AVMA guidelines for humane endpoints and anesthesia-based euthanasia. All experimental protocols used were approved and

implemented in accordance with ethical committees and conformed to the highest international standards for the humane care of animals in biomedical research.

16s DNA extractions and PCR amplification

The DNA was extracted from various samples using the CTAB method following the manufacturer's instructions. The full-length 16S rRNA gene was then amplified using primers 27F: 5'-AGRGTTYGATYMTGGCTCAG-3' and 1492R: 5'-RGYTACCTTGTTACGACTT-3', each tagged with a specific barcode for individual samples. The PCR amplification was carried out in a total reaction volume of 20 μL, which included 4 μL of 5× FastPfu Buffer, 2 μL of 2.5 mM dNTPs, 0.8 μL of each primer (5 μM), 0.4 μL of FastPfu Polymerase, 10 ng of template DNA, and PCR-grade water for volume adjustment. The PCR conditions for amplifying the full-length prokaryotic 16 S rRNA gene included an initial denaturation at 95 °C for 2 min, followed by 25 cycles of denaturation at 95 °C for 30 s, annealing at 55 °C for 30 s, extension at 72 °C for 1 min, and a final extension at 72 °C for 5 min.

Library construction and sequencing

The PCR products were confirmed through 2% agarose gel electrophoresis and subsequently purified using the AxyPrep DNA Gel Extraction Kit (Axygen Biosciences, USA), following the manufacturer's guidelines. After quantification using QuantiFluorTM-ST (Promega, USA), the amplicon pools were prepared for library construction. SMRTbell libraries were created utilizing the Pacific Biosciences SMRTbellTM Template Prep kit 1.0 (PacBio, USA) and sequenced on the PacBio Sequel II platform (LC-Bio Technology Co., Ltd., Hangzhou, China).

Data analysis

We generated Circular Consensus Sequence (CCS) reads from raw subreads using SMRT Link (v6.0) with the following parameters: minPasses = 3; minPredictedAccuracy = 0.99. Subsequently, lima (v1.7.1) was utilized to differentiate CCS reads from different samples, and cutadapt (v1.9) was employed to identify primers. We retained CCS reads that fell within the length range of 1200 bp to 1650 bp after length filtration. After dereplication and the removal of chimeric sequences using DADA2, we obtained a feature table and feature sequences. Alpha diversity and beta diversity were calculated by normalizing to the same sequences randomly.

Alpha diversity was applied to analyze the complexity of species diversity within a sample using 6 indices, including Chao1, Observed-features, Goods coverage, Shannon, Simpson, Pielou-e. All these indices were calculated using QIIME2. Beta diversity was calculated using QIIME2. The Amplicon Sequence Variants (ASVs) were annotated by aligning feature sequences with the SILVA database (release 138). Other diagrams were created using R packages.

Untargeted metabolomics

Liver samples

The collected samples were thawed on ice, and metabolites were extracted using 80% methanol buffer. Briefly, 50 mg of each sample was extracted with 0.5 ml of pre-cooled 80% methanol. The extraction mixture was then stored at -20 °C for 30 min. After centrifugation at 20,000 g for 15 min, the supernatants were tran Supplementary Figure erred into new tubes and vacuum dried. The dried samples were re-dissolved with 100 μL of 80% methanol and stored at -80 °C until LC-MS analysis. Additionally, pooled QC samples were prepared by combining 10 μL from each extraction mixture.

Parameter setting

All samples were acquired using the LC-MS system in the following order: Firstly, all chromatographic separations were performed using an UltiMate 3000 UPLC System (Thermo Fisher Scientific, Bremen, Germany). An ACQUITY UPLC T3 column (100 mm*2.1 mm, 1.8 μm, Waters, Milford, USA) was used for the reversed-phase separation, and the column oven was maintained at 40 °C. The flow rate was set at 0.3 ml/min, and the mobile phase consisted of solvent A (5mM ammonium acetate and 5mM acetic acid) and solvent B (Acetonitrile). Gradient elution conditions were as follows: 0 to 0.8 min, 2% B; 0.8 to 2.8 min, 2–70% B; 2.8 to 5.6 min, 70–90% B; 5.6 to 6.4 min, 90–100% B; 6.4 to 8.0 min, 100% B; 8.0 to 8.1 min, 100–2% B; 8.1 to 10 min, 2% B.

Data analysis

The acquired MS data underwent various pretreatments, including peak picking, peak grouping, retention time correction, second peak grouping, and annotation of isotopes and adducts, all performed using XCMS software. LC – MS raw data files were converted into mzXML format and then processed using XCMS, CAMERA, and the metaX toolbox, implemented with R software. Each ion was identified by combining retention time (RT) and m/z data. The intensities of each peak were recorded, generating a 3D matrix containing arbitrarily assigned peak indices (retention time-m/z pairs), sample names (observations), and ion intensity information (variables).

Metabolite annotation was carried out by matching the exact molecular mass data (m/z) of samples with those in online databases such as KEGG (www.KEGG.jp/KEGG/kegg1.html) and HMDB. Kyoto Encyclopedia of Genes and Genomes (KEGG) Enrichment Analysis (https://www.kegg.jp/kegg/): A KEGG pathway enrichment analysis of differential genes was conducted using the clusterProfiler package, and the results were presented in the form of bubble plots and histograms[29–32]. A mass difference between the observed and database values of less than 10 ppm was used to annotate the metabolite. The molecular formula of metabolites was further identified and validated through isotopic distribution measurements. An in-house fragment spectrum library of metabolites was also used to validate metabolite identification.

The intensity of peak data was further preprocessed using metaX. Features that were detected in less than 50% of QC samples or 80% of biological samples were removed. The remaining peaks with missing values

were imputed using the k-nearest neighbor algorithm to enhance data quality. PCA was performed for outlier detection and batch effects evaluation on the pre-processed dataset. Quality control-based robust LOESS signal correction was applied to the QC data with respect to the order of injection to minimize signal intensity drift over time. Additionally, metabolic features with relative standard deviations > 30% across all QC samples were removed.

Student t-tests were conducted to detect differences in metabolite concentrations between two phenotypes, and the *p*-values were adjusted for multiple tests using the Benjamini–Hochberg False Discovery Rate (FDR) method. Supervised PLS-DA was performed through metaX to discriminate different variables between groups. A VIP value cutoff of 1.0 was used to select important features. We adopted VIP value > 1 as the screening threshold, as metabolites with VIP values exceeding 1 generally exhibit higher biological relevance. This criterion aligns with the majority of comparable studies and is widely employed in metabolomics research to effectively identify metabolites that make significant contributions to model predictions.

Untargeted lipidomics

Liver samples

The collected samples were thawed on ice, and metabolites were extracted using a lipid extraction buffer. In brief, 100 mg of sample was mixed with 1 ml of pre-cooled lipid extraction buffer (IPA: ACN: H2O = 2:1:1), followed by vortexing for 1 min and incubation at room temperature for 10 min. The extraction mixture was then stored overnight at -20 °C. After centrifugation at 4,000 g for 20 min, the supernatants were transferred into new 96-well plates. These samples were subsequently stored at -80 °C until the LC-MS analysis. Additionally, pooled QC samples were prepared by combining 10 µL from each extraction mixture.

Parameter setting

All samples were acquired by the LC-MS system followed machine orders. Firstly, all chromatographic separations were performed using an ACQUITY UPLC System (Waters, Milford, MA, USA). A Kinetex UPLC C18 column (100 mm*2.1 mm, 100 A, phenomenex, UK) was used for the reversed phase separation. The column oven was maintained at 55 °C. The flow rate was 0.3 ml/min and the mobile phase consisted of solvent A (ACN: H2O = 6:4, 0.1% formic acid) and solvent B (IPA: ACN = 9:1, 0.1% formic acid). Gradient elution conditions were set as follows: 0 ~ 0.4 min, 30% B; 0.4 ~ 1 min, 30–45% B;1 ~ 3 min, 45–60% B; 3.5 ~ 5 min,60–75% B; 5 ~ 7 min, 75–90% B; 7 ~ 8.5 min, 90–100% B; 8.5 ~ 8.6 min, 100% B; 8.6 ~ 8.61 min, 100–30% B; 8.61 ~ 10 min, 30%B.

Data analysis

A high-resolution tandem mass spectrometer, TripleTOF 6600 (SCIEX, Framingham, MA, USA), was employed to detect metabolites eluted from the column. The Q-TOF operated in both positive and negative ion modes. The curtain gas was set at 30 PSI, Ion source gas 1 and Ion source gas 2 were both set at 60 PSI, and the interface heater temperature was maintained at 650 ℃. In the positive ion mode, the Ionspray voltage was set at 5000 V. For the negative ion mode, the Ionspray voltage was set at -4500 V. Mass spectrometry data were acquired in IDA mode, with the TOF mass range spanning from 60 to 1200 Da. The survey scans were collected in 150 ms intervals, and up to 12 product ion scans were obtained if they exceeded a threshold of 100 counts per second (counts/s) with a 1 + charge-state. The total cycle time was fixed at 0.56 s. Four times bins were summed for each scan at a pulser frequency value of 11 kHz, monitored through the 40 GHz multichannel TDC detector with four-anode/channel detection. Dynamic exclusion was set for 4 s. Calibration for mass accuracy was performed every 20 samples during acquisition. Additionally, to assess the stability of the LC-MS throughout the acquisition, a QC sample (Pool of all samples) was acquired after every 10 samples.

ELISA

The serum samples were tested using a commercially available rat ELISA kit (D731062-0096, Sangon, Shanghai, China). In a 96-well plate pre-coated with antibodies, standard sample wells, blank wells, and detection sample wells were set up. In the detection wells (triplicates), 50 µL of rat serum was added to the bottom of each well. After sealing the plate with a sealing membrane, it was incubated at 37 °C for 30 min. The sealing membrane was then removed, and the liquid was discarded. The plate was dried and subjected to 5 repeated washes with a washing solution. After the washing steps, 50 µL of enzyme-labeled reagent was added to each well (except for the blank wells). The plate was incubated at 37 °C for 30 min and then washed again. Subsequently, 50 µL of chromogenic reagent A and 50 µL of chromogenic reagent B were added to each well. The plate was gently shaken to mix the contents, and then incubated at 37 °C in the dark for 10 min. Finally, 50 µL of stop solution was added to each well to terminate the reaction. The absorbance (OD value) of each well was measured sequentially at a wavelength of 450 nm, with the blank well serving as the reference. A standard curve was established using the concentrations and OD values of the standard samples. After determining the linear regression equation of the standard curve, the concentrations of the analytes in the detection samples were calculated (averaged from triplicates).

Statistics and reproducibility

Statistical significance was calculated with R project (https://www.r-project.org/). Multiple comparisons were performed using a one-way ANOVA test with post hoc Tukey test, unless stated otherwise. The correlation between parameters was analyzed using a correlation t test. Values of $p < 0.05$ were considered statistically significant.

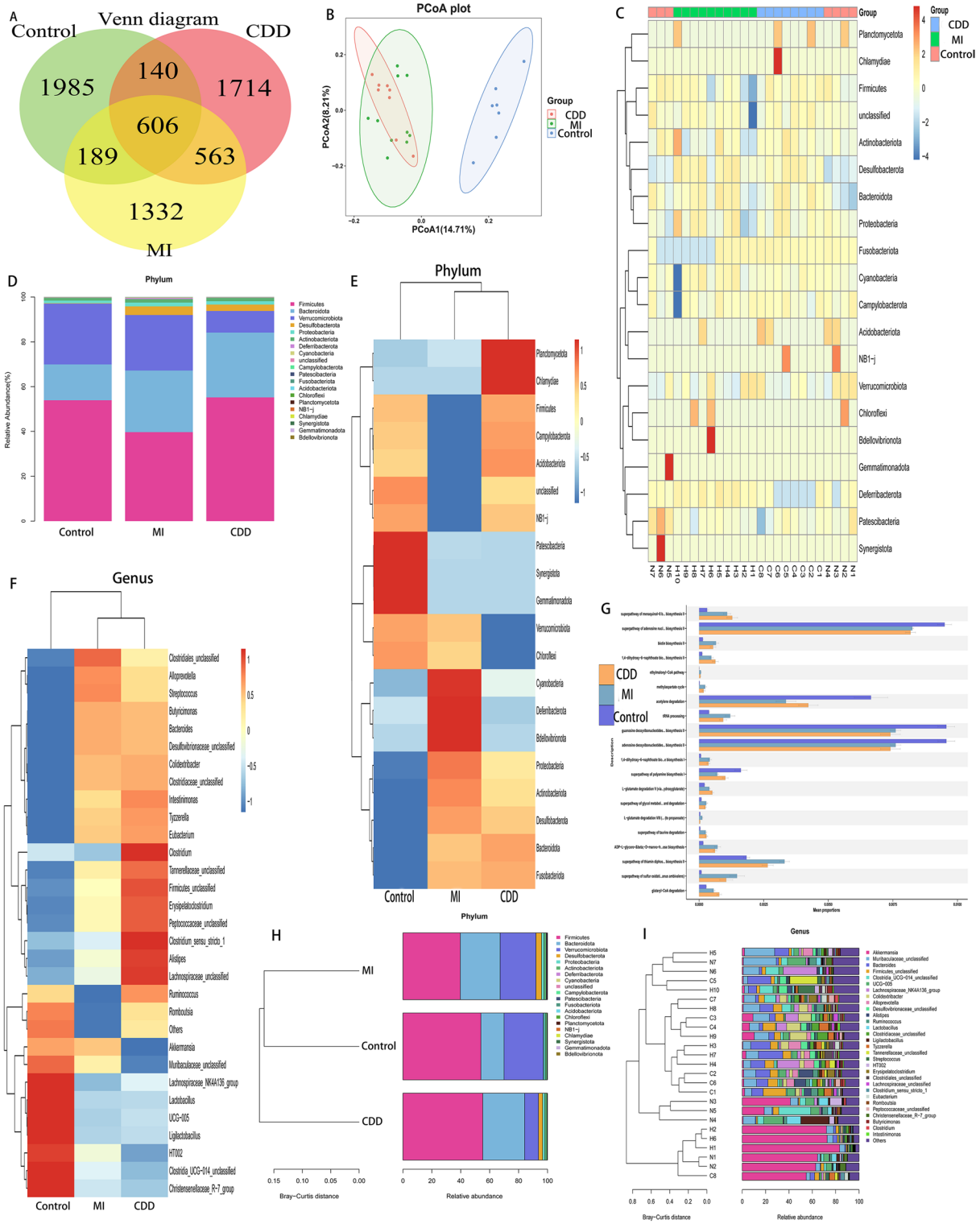

Results

General changes in the ending

We successfully gathered complete data from 25 rats, divided into three groups: 7 in the Control group (fed with a normal diet), 8 in the CDD group (fed with a choline-deficient diet), and 10 in the MI group (choline-deficient diet with metformin intervention). Compared to the control group, the two experimental groups exhibited significant changes in their liver appearance and liver weight ratio (LWR) (Fig. 1B and D). The liver-to-body weight ratio in rats from the CDD group showed significant differences compared to both the MI group and the Control group. However, there were no statistically significant differences between the MI group and the Control group. The Lee's index among the three groups of rats did not show any significant statistical differences (Fig. 1C). Representative images of liver Masson's trichrome staining and Oil Red O staining are shown in Fig. 1E.

◀**Fig. 2**. Comparative analysis of gut microbial diversity and expression abundance in rats. (**A**) Number of shared or unique Operational Taxonomic Units (OTUs) across different groups; (**B**) Unweighted Unifrac PCoA plot illustrating the gut microbial composition in various rat groups; (**C**) The top 30 most abundant phyla in the gut microbiota of different rat groups; (**D**) Comparison of sample abundance and dominant species in the top 20 most abundant phyla in rat gut microbiota; (**E**) Normalized comparison of microbial abundance expression at the phylum level in rats; (**F**) Normalized comparison of microbial abundance expression at the genus level in rats; (**G**) STAMP analysis of the expression abundance of rat microbial abundance based on PICRUSt2 functional predictions; (**H**) Cluster analysis of gut microbial groups in rats at the phylum level; (**I**) Cluster analysis of gut microbiota per sample in rats at the genus level. Con/Control: control group with standard diet; CDD: choline-deficient high-fat diet group; MI: metformin-treated choline-deficient high-fat diet group; OTU: Operational Taxonomic Units; p-values obtained via two-tailed unpaired Student's t-tests; $^{*}p < 0.05$; $^{**}p < 0.01$; $^{***}p < 0.001$; $^{****}p < 0.0001$; ns: no significance.

Analysis of blood samples from the rats indicated the presence of liver damage and chronic inflammation in both the MI and CDD groups (Fig. 1F). The levels of AST (Aspartate Aminotransferase) and ALT (Alanine Aminotransferase) were higher in rats from both the CDD and MI groups compared to the Control group. However, no differences were observed between the CDD and MI groups. In the blood sample tests for total bilirubin (TBIL), the levels in rats from the CDD group were significantly higher than those in the Control group, while the MI group did not show abnormal TBIL levels. The test results for ALP (Alkaline Phosphatase) also showed a similar trend. The data suggest that metformin may have a protective effect on the liver, but this effect may not be pronounced. We have discerned that metformin can play a role in delaying liver fibrosis. Pathological results indicate that, although the rats in the metformin group also showed a tendency towards liver fibrosis, the degree of liver damage and the severity of fibrosis were lower than those in the CDD group. Serum levels of ALT and AST also revealed that the liver function impairment in the metformin-treated rats did not significantly differ from that in the untreated MAFLD rats. This could be due to the severity of liver damage induced by the MAFLD modeling, suggesting that even if metformin has some therapeutic effect, it might not be sufficient to create a significant difference at the biochemical marker level. Hence, we can observe that metformin has a certain capacity to maintain normal liver function and slow the progression of fibrosis related to MAFLD. However, our findings diverge from those of other researchers regarding metformin's ability to reduce liver damage, indicating that further clarification is needed to fully ascertain its efficacy.

Fecal microbiome composition analysis

The raw sequencing data were analyzed using QIIME2, and Venn diagrams were utilized to display the overlaps and uniqueness of Operational Taxonomic Units (OTUs) among the three groups. The data were clustered into OTUs based on 97% similarity. The Venn diagram in Fig. 2A illustrates that 606 OTUs were identified across all groups. The unique number of OTUs in the Control, CDD, and MI groups were 1985, 1714, and 1332, respectively. Additionally, 140 OTUs were identified in both the Control and CDD groups, 189 OTUs in both the Control and MI groups, and 563 OTUs in both the CDD and MI groups. These findings suggest that the diversity of the gastrointestinal microbiota in MAFLD rats is lower than in normal rats, and the intervention with metformin appears to further reduce the diversity of the gastrointestinal microbiota.

Beta diversity was utilized to measure the phylogenetic distance between bacterial communities in each sample (Fig. 2B). The figure displays a Principal Coordinates Analysis (PCoA) of the 16 S rRNA dataset. Each point on the graph represents the entire bacterial community within a sample. Samples that are closer together have similar microbial community compositions, while those further apart are less alike. We observed that each group in the collected fecal samples displayed distinct bacterial taxa, indicating that both MAFLD induced by a choline-deficient diet and metformin intervention lead to alterations in the composition of the gut microbiome. The top 30 most abundant phyla are enumerated and illustrated using a heatmap (Fig. 2C). A stacked bar chart lists these 30 most abundant phyla (Fig. 2D), and the top 30 phyla and genera are presented in the form of heatmaps (Fig. 2E and F). The heatmap displays the 30 most abundant phyla in the samples. The abundance of each phylum is typically represented by the intensity of the color; a darker color signifies a higher relative abundance of that phylum in a specific sample.

To characterize the gut microbiota of MAFLD rats, we examined the taxonomic composition and relative abundance of microbial communities in feces at different taxonomic levels. At the phylum level, the three groups generally displayed similar dominant phyla, with "*Firmicutes*," "*Bacteroidota*," and "*Verrucomicrobiota*" being predominant in the gut microbiota of all sampling groups. This is consistent with previous studies on gut microbial composition. Although the composition of the dominant phyla in the gut of rats from different groups was similar, differences in relative abundance were observed among the three phyla. Specifically, we noted that the relative abundance of Firmicutes was similar in the Control and CDD groups of rats, but significantly decreased in the intestines of rats subjected to metformin intervention. Conversely, the relative abundance of "*Bacteroidota*" significantly increased in the intestines of rats with MAFLD (Fig. 2D). In the intestines of the control group and rats treated with metformin, the abundance of "*Verrucomicrobiota*" was similar, while in rats with MAFLD not subjected to drug intervention, the abundance of "*Verrucomicrobiota*" was significantly decreased.

In our study, we observed a progressive increase in the abundance of "*Alistipes*", "*Desulfovibrionaceae*", "*Tyzzerella*", "*Peptococcaceae*" across the spectrum from healthy rats to MAFLD rats treated with metformin, and then to untreated MAFLD rats. In contrast, the levels of "*Akkermansia*", "*Ligilactobacillus*", "*Lactobacillus*", "*UCG-005*", "*HT002*", "*Clostridia-UCG-014*", and the "*Christensenellaceae-R-7*" group significantly decreased in the gut

microbiota of MAFLD rats compared to healthy rats. Notably, in the intestines of rats treated with metformin, some specific microbial classes, including "*Alistipes*", "*Firmicutes*", "*Tannerellaceae*", and "*Ruminococcus*", exhibited a unique declining trend.

Based on the PICRUSt2 functional prediction outcomes, the STAMP analysis focused on the top 30 pathways with significant differences ($p < 0.05$) in the t-test comparisons between groups, with these differences visually represented in images (Fig. 2G). These results displayed functions with statistically significant differences (95% confidence interval). In MAFLD rats, certain pathways like the 'superpathway of polyamine biosynthesis,' 'acetylene degradation,' 'superpathway of adenosine nucleotides de novo biosynthesis II,' 'guanosine deoxyribonucleotides de novo biosynthesis II,' and 'adenosine deoxyribonucleotides de novo biosynthesis II' exhibited a notable decrease. In contrast, pathways such as 'biotin biosynthesis II,' '1,4-dihydroxy-6-naphthoate biosynthesis II,' 'superpathway of menaquinol-8 biosynthesis II,' 'tRNA processing,' 'ADP-L-glycero-β-D-manno-heptose biosynthesis,' 'superpathway of thiamin diphosphate biosynthesis II,' 'superpathway of sulfur oxidation (Acidianus ambivalens),' and 'glutaryl-CoA degradation' in MI group were significantly more active.

In the analysis using the KEGG dataset (http://www.KEGG.jp/KEGG/kegg1.html) (Supplementary Fig. 1A, Supplementary Fig. 1A), it was observed that in MAFLD rats, pathways such as 'Pertussis,' 'Meiosis - yeast,' 'Biosynthesis and biodegradation of secondary metabolites,' 'Phenylalanine metabolism,' 'Novobiocin biosynthesis,' 'Tropane, piperidine, and pyridine alkaloid biosynthesis,' 'Isoquinoline alkaloid biosynthesis,' and 'Histidine metabolism' showed a significant increase. Conversely, pathways like 'Biosynthesis of unsaturated fatty acids,' 'Tuberculosis,' 'Signal transduction mechanisms,' 'Base excision repair,' 'Photosynthesis,' and 'Photosynthesis proteins' exhibited a notable decrease.

In the analysis using the Clusters of Orthologous Groups (COG) dataset (Supplementary Fig. 1B), it was observed that in MAFLD rats compared to the control group, the expression of 'Xanthine/uracil/vitamin C permease, AzgA family' was significantly reduced. On the other hand, several other genes showed increased activity. These include 'Antirestriction protein ArdC,' 'Methylaspartate ammonia-lyase,' 'DNA-binding transcriptional response regulator, NtrC family, containing REC, AAA-type ATPase, and Fis-type DNA-binding domains,' 'tRNA C32,U32 (ribose-2'-O)-methylase TrmJ or a related methyltransferase,' 'Predicted dienelactone hydrolase,' 'Dissimilatory sulfite reductase (desulfoviridin), alpha and beta subunits,' 'Mg2 + and Co2 + transporter CorB, containing DUF21, CBS pair, and CorC-HlyC domains,' and 'Sensor histidine kinase regulating citrate/malate metabolism.' These changes in gene activity suggest alterations in various metabolic and regulatory pathways in the gut microbiome of MAFLD rats, highlighting the potential impacts of the disease on different biological processes. This information is vital for understanding the pathophysiology of MAFLD and could guide future research into therapeutic strategies.

Then, we used the Bray-Curtis distance for clustering analysis of the microbiota at the genus level. The results (as shown in Fig. 2H and Supplementary Fig. 1C) revealed similarities within the microbial communities of MAFLD rats, and notably, these communities were significantly different from those in normal rats. The Bray-Curtis distance, a measure used to quantify the compositional dissimilarity between two different sites or conditions based on counts at each site, effectively highlighted the differences in microbial composition between the MAFLD and normal rats. This analysis is crucial for understanding how MAFLD affects gut microbiota composition, which could have implications for the disease's pathogenesis and potential treatment strategies. It is noteworthy that in both groups of MAFLD rats, there was a significant increase in the presence of the *Desulfobacterota* phylum, whereas this phylum was not observed in the intestines of normal rats. The presence and increase of *Desulfobacterota* in MAFLD rats suggest a potential association between this phylum and the pathophysiology of MAFLD. *Desulfobacterota*, known for its involvement in sulfate reduction and other metabolic processes, could play a role in the altered gut microbiome environment seen in MAFLD. This finding provides valuable insights into the gut microbiota's alterations in MAFLD and its potential impact on disease progression, offering possible avenues for further research and therapeutic intervention.

In the genus-level clustering analysis results (Fig. 2I), an intriguing observation was the significant increase in the presence of genera such as '*Akkermansia*', '*Alloprevotella*', '*Alistipes*', '*Bacteroides*', '*Tyzzerella*', and '*Colidextribacter*' in the intestines of MAFLD rats. The increased abundance of these genera in MAFLD rats indicates significant changes in the gut microbial community that could be linked to the pathogenesis or effects of MAFLD.

The significant barplot difference analysis involved a differential analysis of all microbial species across all samples (Fig. 3A). This analysis filtered out the top 30 most abundant microbes (at the genus level) with a p-value < 0.05 and displayed them in a bar chart. In this chart, the horizontal axis represents the different species, arranged from left to right based on their abundance, while the vertical axis indicates their relative abundance. In MAFLD rats, there was a notable increase in the abundance of several genera, including '*g__Bacteroides*,' '*g__Firmicutes_unclassified*,' '*g__Colidextribacter*,' '*g__Alloprevotella*,' '*g__Desulfovibrionaceae_unclassified*,' '*g__Clostridiales_unclassified*,' '*g__Tyzzerella*,' and '*g__Tannerellaceae_unclassified*.' In MAFLD rats, there was a significant decrease in the abundance of several genera, including '*g__Clostridia_UCG-014_unclassified*,' '*g__UCG-005*,' '*g__Lactobacillus*,' '*g__HT002*,' '*g__Christensenellaceae_R-7_group*,' '*g__[Eubacterium] coprostanoligenes_group_unclassified*,' '*g__Muribaculum*,' '*g__Prevotellaceae_UCG-001*,' '*g__Prevotellaceae_NK3B31_group*,' and '*g__[Eubacterium]_siraeum_group*'.

Figure 3B illustrates the species annotation information at the genus level and their relative abundance (indicated by the size of circles) across different sample groups. Additionally, the figure also displays the species annotation information corresponding to their phylum (indicated by the color of the circles). In MAFLD rats, genera such as '*Bacteroides*,' '*Colidextribacter*,' '*Streptococcus*,' and '*Tyzzerella*' showed increased activity, whereas '*UCG-005*,' '*Akkermansia*,' '*HT002*,' '*Lactobacillus*,' and '*Ligilactobacillus*' exhibited a decrease in their presence. Interestingly, in MAFLD rats treated with metformin, the genera '*Alistipes*' and '*Akkermansia*' demonstrated expression levels similar to those in normal rats.

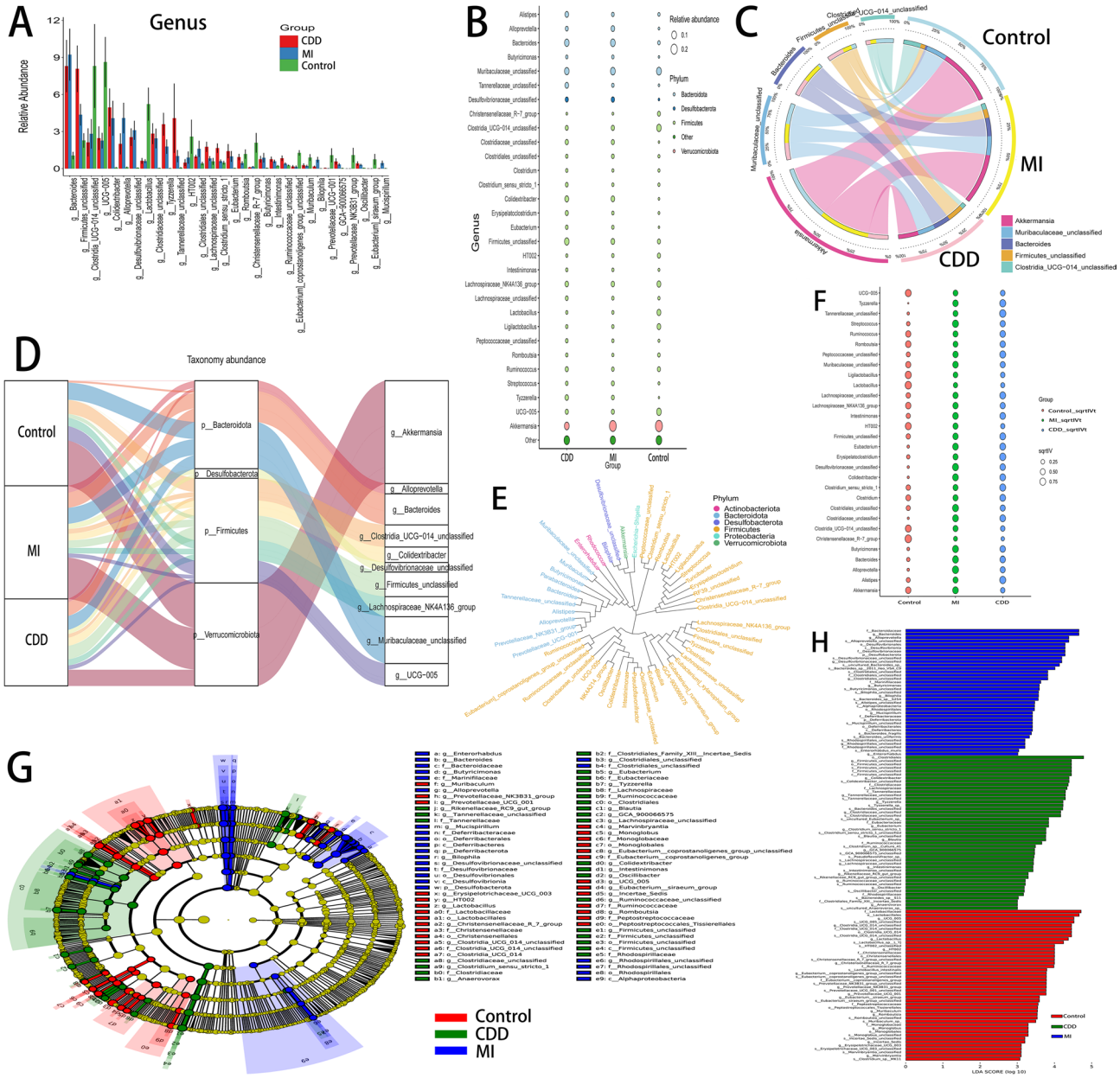

Fig. 3. Changes in gut microbial species and expression abundance in rats. (**A**) Significant differences in the top 20 most abundant species across groups at the genus level; (**B**) Species annotation information and relative abundance at the genus level in different sample groups; (**C**) Top 5 phyla in microbial abundance and their corresponding abundance information; (**D**) Relative abundance of microbial communities at phylum (middle) and genus (right) levels for different group samples (left); (**E**) Evolutionary tree of top 50 genus-level species in microbial expression abundance; (**F**) Comparison of sqrtIVt values for microbial indicator value at the genus level; (**G**) Evolutionary branching diagram for seven taxonomic levels (kingdom, phylum, class, order, family, genus, species), with each node representing a species classification. Larger nodes indicate higher species abundance. Yellow nodes indicate no significant difference in species between comparison groups, red nodes indicate significant differences with higher abundance in the red group, and so on. Significant differences in phyla are directly labeled in the diagram, and other levels are indicated by letters; (**H**) Bar chart showing biomarkers with significant differences (LDA score > 3.0), where the color of the bars represents which group the species is more abundant in, and the length indicates the LDA score, reflecting the extent of difference between groups. Con/Control: control group with standard diet; CDD: choline-deficient high-fat diet group; MI: metformin-treated choline-deficient high-fat diet group; p-values obtained via two-tailed unpaired Student's t-tests; $^{*}p < 0.05$; $^{**}p < 0.01$; $^{***}p < 0.001$; $^{****}p < 0.0001$; ns: no significance.

The top five most abundant phyla in the gut microbiota of different rat models, along with their corresponding abundance information, are depicted in Fig. 3C. The width of each segment reflects the abundance level: wider segments indicate higher abundance, while narrower segments signify lower abundance. Notably, '*Akkermansia*' constitutes the highest proportion (usually around 50%) in the intestines of normal rats and those treated with metformin. However, this proportion significantly declines in the intestines of untreated MAFLD rats. In contrast, '*Clostridia_UCG-014_unclassified*' shows a marked decrease in the intestines of MAFLD rats, with a severe reduction in abundance compared to normal rats, regardless of drug intervention. Conversely, '*Firmicutes_unclassified*' significantly increases in the intestines of MAFLD rats. While metformin intervention reduces its abundance to some extent, it still exhibits an unusually high trend compared to normal rats. This visual representation underscores the significant shifts in gut microbiota composition associated with MAFLD and its modulation by metformin treatment.

We also employed Fig. 3D to render the compositional differences of the microbiota in each group more pronounced. We have defaulted to selecting the top 50 genera based on abundance for constructing the Fig. 3E plot. Within this plot, distinct branches represent different genera-level classifications. Genera of different types but sharing the same color indicate that they belong to the same phylum. The closer the proximity between any two species, the more closely related they are evolutionarily. This allows for an intuitive understanding of the phylogenetic relationships and biological significance of the species under focused study.

The square root of the indicator value (sqrtIVt) is utilized to compare the magnitude of association between microbes and each group under different treatment strategies, thereby revealing potential gut microbiota biomarkers for the progression of MAFLD and metformin intervention. The computational results indicate significant differences between MAFLD and non-MAFLD rats in genera such as '*Tyzzerella*', '*Tannerellaceae*', '*Desulfovibrionaceae*', '*Eubacterium*', '*Colidextribacter*', '*Clostridiaceae*', '*Clostridiales*', '*Butyricimonas*', '*Bacteroides*', and '*Alloprevotella*'. In the MAFLD rat model, '*Akkermansia*', '*HT002*', '*Clostridiales*', and '*Alloprevotella*' demonstrated dominance in the feces of rats not treated with metformin, whereas their expression dominance was somewhat suppressed post-metformin intervention (Fig. 3F). '*Akkermansia*', '*Clostridiales*', and '*Alloprevotella*' exhibited similar expression levels in the control non-MAFLD rat model and under the influence of metformin in the MAFLD rat model. Notably, they showed a clear advantage in the intestines of severely MAFLD-affected rats without intervention, suggesting their potential as biomarkers.

The phylogenetic branching diagram obtained from the LEfSe differential analysis corroborates the results of the prior analyses from an additional perspective. Notably, a significant divergence is observed in the MAFLD rat post-pharmacological intervention, where '*g_Clostridium_sensu_stricto_1*', '*f_Bacteroidaceae*', '*f_Marinifilaceae*', '*p_Deferribacterota*', and '*p_Desulfobacterota*' demonstrate a predominance in species abundance within the intestinal tract of these rats (Fig. 3G). This suggests that Metformin may exert a discernible impact on these microbial taxa. Figure 3H indicates microbial species abundances surpassing the anticipated LDA scores, with '*f_Bacteroidaceae*' and '*g_Bacteroides*' exhibiting substantial alterations following drug intervention. Together with '*g_Alloprevotella*', they may serve as significant biomarkers for Metformin's intervention in MAFLD. Conversely, in untreated MAFLD rats, the computational outcomes seem to favor Clostridiales and Firmicutes as biomarkers for the progression of MAFLD to severe liver fibrosis. For the pairwise comparative groups, differential analysis of ASV abundance was conducted. In Figs. 4A–C, 'enriched' (upper triangle) denotes a significant upregulation, 'depleted' (lower triangle) signifies a significant downregulation, and 'nosig' (dot) indicates no significant difference. Different colors are used to distinguish the phylum-level taxa to which each ASV belongs.

By calculating the abundance of the top 30 genera, we obtained the correlations and significant p-values between each pair of dominant microbial communities. Subsequently, a network diagram (Supplementary Fig. 1D) was constructed using Spearman's correlation results for relationships where $|rho| > 0.8$. In our study, a pronounced symbiotic relationship was evident between '*Colidextribacter*' and '*Tyzzerella*', as well as between '*Firmicutes_unclassified*' and '*Lachnospiraceae_unclassified*'. The heatmap in Fig. 4D illustrates the interrelations among various microorganisms.

Mapping the functional predictions from PICRUSt2 to the analysis obtained from the GEO database reveals significant functional discrepancies among normal rats, metformin-treated MAFLD rats, and untreated MAFLD rats. Key proteins and systems, including 'Antirestriction protein ArdC', 'Dissimilatory sulfite reductase (desulfoviridin), alpha and beta subunits', 'Site-specific recombinase XerC', 'ABC-type uncharacterized transport system involved in gliding motility, auxiliary component', 'Mg2 + and Co2 + transporter CorB, containing DUF21, CBS pair, and CorC-HlyC domains', and 'Sensor histidine kinase regulating citrate/malate metabolism,' exhibited marked functional variations, demonstrating a distinct and progressive upward trend (Fig. 4E). This trend underscores the nuanced shifts in metabolic and regulatory pathways induced by metformin treatment and disease progression in MAFLD rats. Corresponding with the aforementioned analysis, in MAFLD rats treated with metformin, there was a notable increase in the expression of 'DNA-binding transcriptional response regulator, NtrC family, contains REC, AAA-type ATPase, and a Fis-type DNA-binding domains', 'Methylaspartate ammonia-lyase', 'tRNA C32,U32 (ribose-2'-O)-methylase TrmJ or a related methyltransferase', 'Predicted dienelactone hydrolase', 'Intracellular sulfur oxidation protein, DsrE/DsrF family', '23S rRNA U2552 (ribose-2'-O)-methylase RlmE/FtsJ', and '3-oxoacyl-[acyl-carrier-protein] synthase III' compared to normal rats and untreated MAFLD rats. These alterations might be intricately linked to the potential role of metformin in decelerating the progression of MAFLD and liver fibrosis. The observed elevations in these specific metabolic and regulatory pathways highlight the possible mechanistic connections between metformin treatment and its therapeutic effects in mitigating MAFLD and its associated pathologies. Finally, in the control group of healthy rats, a significantly higher expression of 'Xanthine/uracil/vitamin C permease, AzgA family' was observed compared to all MAFLD rats, whether treated or not. This suggests a potential inhibitory role associated with the progression of MAFLD. The marked distinction in expression levels indicates that this permease could be intricately linked to mechanisms that mitigate or resist the advancement of MAFLD. The 'AzgA family' of

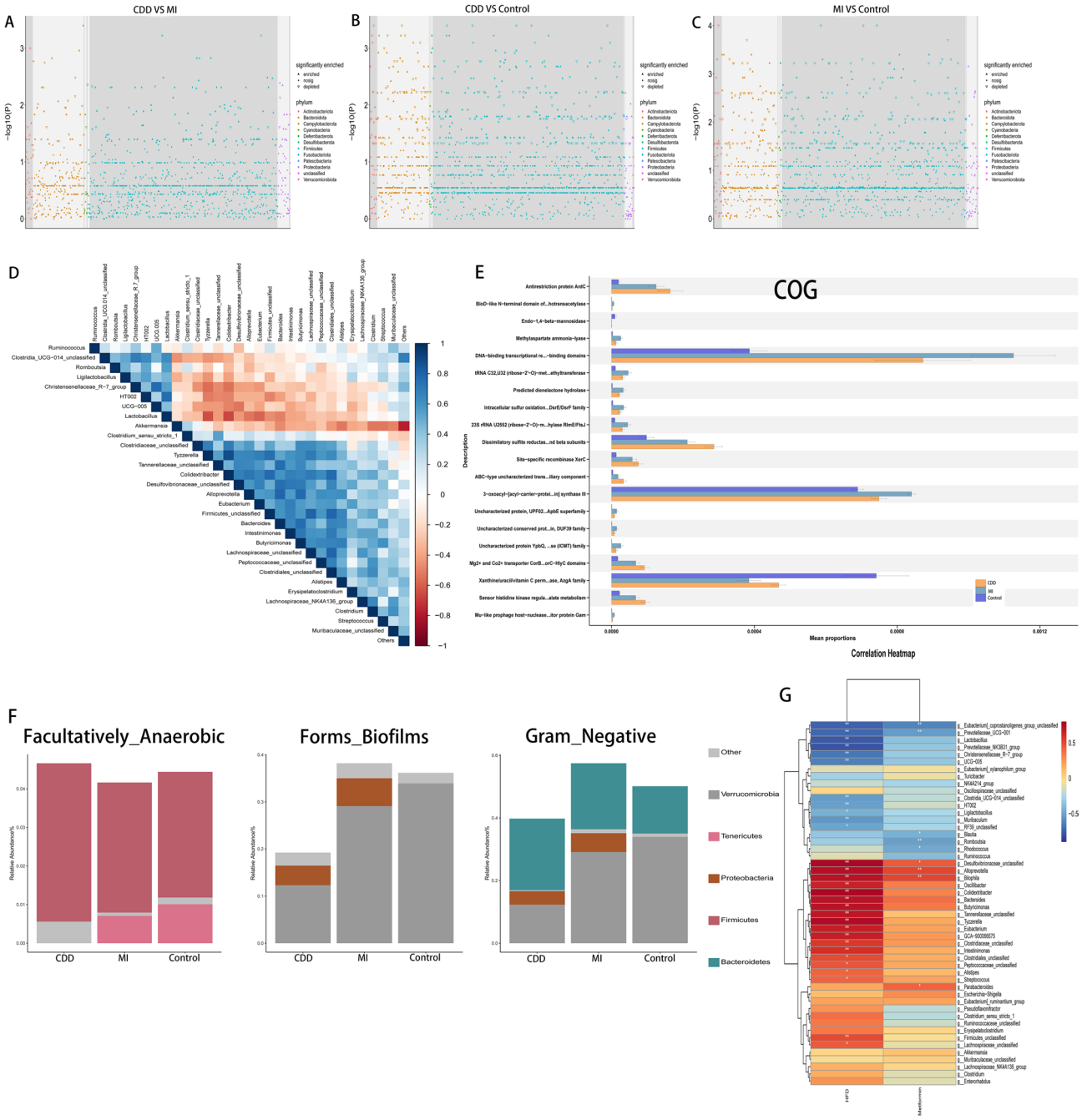

Fig. 4. Comparative Analysis of Gut Microbial Diversity and Expression Abundance in Rats. (**A**) ASV abundance differences between CDD and MI groups, with enriched (upward triangle) indicating significant upregulation, depleted (downward triangle) indicating significant downregulation, and nosig (dot) for no significant difference, differentiated by colors representing phylum-level species; (**B**) ASV abundance differences between CDD and control groups, with enriched, depleted, and nosig symbols, and color differentiation at the phylum level; (**C**) ASV abundance differences between MI and control groups, similarly indicated and color-coded; (**D**) Top 30 genus-level microbial abundance Spearman correlation analysis, showing correlations and significant p-values between dominant microbial groups; (**E**) Functional prediction STAMP difference analysis (annotated using COG database); (**F**) Column stacked chart showing relative abundance of species with different phenotypes (Facultatively Anaerobic, Forms Biofilms, Gram Negative) in various groups; (**G**) Spearman correlation coefficients between microbiota and environmental indicators, displayed as a cluster heatmap, with red indicating positive correlation and blue indicating negative correlation. Deeper colors signify stronger correlations. Con/Control: control group with standard diet; CDD: choline-deficient high-fat diet group; MI: metformin-treated choline-deficient high-fat diet group; ASV: Amplicon Sequence Variants; p-values obtained via two-tailed unpaired Student's t-tests; $^{*}p < 0.05$; $^{**}p < 0.01$; $^{***}p < 0.001$; $^{****}p < 0.0001$; ns: no significance.

proteins, by regulating the transport of nucleotides and vitamin C, may impact cellular energy balance and redox status. These factors are critical regulators of fatty acid synthesis and degradation. By modulating the availability and metabolism of nucleotides and ascorbic acid, 'AzgA proteins' potentially influence key biochemical pathways that dictate the synthesis and breakdown of fatty acids, pivotal processes in maintaining cellular health and metabolic homeostasis.

Subsequently, we employed BugBase to predict nine potential phenotypes, including Aerobic, Anaerobic, Contains Mobile Elements, Facultatively Anaerobic, Forms Biofilms, Gram Negative, Gram Positive, Potentially Pathogenic, and Stress Tolerant. This predictive analysis allows for a comprehensive understanding of the microbial community's functional capabilities and potential impacts on the host environment. By characterizing these phenotypes, we can infer important aspects of microbial behavior, interaction, and overall impact on the ecosystem or host. Through meticulous analysis and screening of our results, we have chosen to present only the most significant outcomes from three analyses: Facultatively Anaerobic, Forms Biofilms, and Gram Negative (Fig. 4F). In the analysis of Facultatively Anaerobic, we observed a stark contrast in the expression of Tenericutes in the gut of rats with severe MAFLD, where it dropped to zero, while maintaining an abundance of over 0.05 in both the control group and the treated MAFLD rats. In the cases of Forms Biofilms and Gram Negative, there was a notable increase in the abundance of Proteobacteria expression in MAFLD rats, while no expression was detected in the control group for Proteobacteria. These findings highlight the distinct microbial shifts associated with the condition and potentially offer insights into the pathophysiological mechanisms underlying MAFLD.

To ascertain the specific effects of metformin on the gut microbiota, we once again utilized the Spearman Correlation Coefficient to compute the correlation between metformin and various gut microorganisms. The relationships were then depicted in the form of a clustering heatmap (Fig. 4G), allowing us to visualize and discern the intricate interactions between metformin and the gut microbiome. In the correlational cluster analysis, it is evident that metformin has influenced the abundance of certain microbes in the rat gut, displaying a significant positive or negative correlation with the usage of the drug. This observation highlights the discernible impact of metformin on the gut microbial composition, suggesting a direct or indirect interaction between the medication and the microbial community. After the administration of metformin, there was a notable decrease in the relative abundance of '*g__Desulfovibrionaceae_unclassified*', '*g__Alloprevotella*', '*g_Bilophila*', '*g_Blautia*', '*g_Romboutsia*', and '*g_Rhodococcus*'. Conversely, '*g_Eubacterium_coprostanoligenes_group*', '*g__Prevotellaceae_UCG_001*', and '*g_Parabacteroides*' exhibited a significant increase in abundance under the influence of the drug. These shifts in microbial populations reflect the substantial impact of metformin on the gut microbiome's composition and dynamics.

Untargeted metabolomic analysis

Supplementary Fig. 3 and Supplementary Table 1 presents the Total Ion Chromatogram (TIC) and the distribution of metabolites in terms of m/z-retention time (rt) for metabolomics. By comparing the liver samples of two groups of MAFLD rats, it is evident that metformin effectively inhibits abnormal fat deposition in the liver (see Fig. 5A). Following the administration of metformin, over a thousand alterations were observed in the hepatic metabolites of MAFLD rats, suggesting that the liver metabolic patterns have also shifted in response to the drug's influence. Notably, the number of metabolic ions both upregulated and downregulated after metformin treatment is considerably substantial. This suggests that both the progression of MAFLD and the treatment with metformin significantly impact the local metabolic patterns in the rat liver. A total of 56,471 metabolites have been positively identified in the liver samples, primarily involved in lipids and lipid-like molecules, organoheterocyclic compounds, organic oxygen compounds, and organic acids and derivatives (Supplementary Fig. 4A, Table 1). The metabolic analysis results, mapped onto the KEGG pathway classification chart (Supplementary Fig. 4B), indicate a significant correlation between the metabolites and the pathways involved in the onset and progression of human tumors. Furthermore, these metabolites are predominantly associated with the pathways of the digestive and endocrine systems. Specifically, within these metabolic pathways, the metabolites demonstrate substantial relevance to Global and overview maps, Amino acid metabolism, Carbohydrate metabolism, Lipid metabolism, and the Metabolism of cofactors and vitamins.

PCA (Principal Component Analysis) of the identified metabolic ions reveals each point in the graph as a representation of an individual sample, with the similarities and differences among all samples manifested through the separation and clustering trends observed in the plot. The aggregation of points indicates a high degree of similarity among the observed variables. Quality Control (QC) results demonstrate good consistency throughout the sample analysis process. The PCA results show distinct separation among the three groups under both positive and negative ion modes (Fig. 5B). These findings suggest a biochemical dysregulation in the serum of MAFLD rats, with a marked alteration in metabolic patterns. PLS-DA indicates significant metabolic differences between the three groups, signifying that metformin has a substantial impact on the hepatic metabolism of rats (Fig. 5C). Figures 5D-F present the PLS-DA score plots for pairwise comparisons among the three groups, along with permutation tests and volcano plots of differential metabolites. From the permutation plots, it can be observed that all three comparison models exhibit no overfitting, as indicated by all Q2 values being less than 0. This suggests that the models are robust and the identified differences in metabolites between the groups are statistically valid and not a result of model overfitting.

Comparative analysis of the differential substances' expression across samples from different groups is visualized using a heatmap, where the intensity values of each metabolite have been normalized. The group clustering analysis results (Supplementary Fig. 2) reveal significant differences in untargeted metabolism pathways between the three groups of rats, indicating changes in metabolic patterns among them. From the overview provided in Fig. 5G, it is evident that there are classifiable changes in metabolite substances among the three groups, and these alterations are statistically significant. Figure 5H presents a pathway map involving secondary identified metabolites, with the top 20 pathways represented on the horizontal axis and the number of

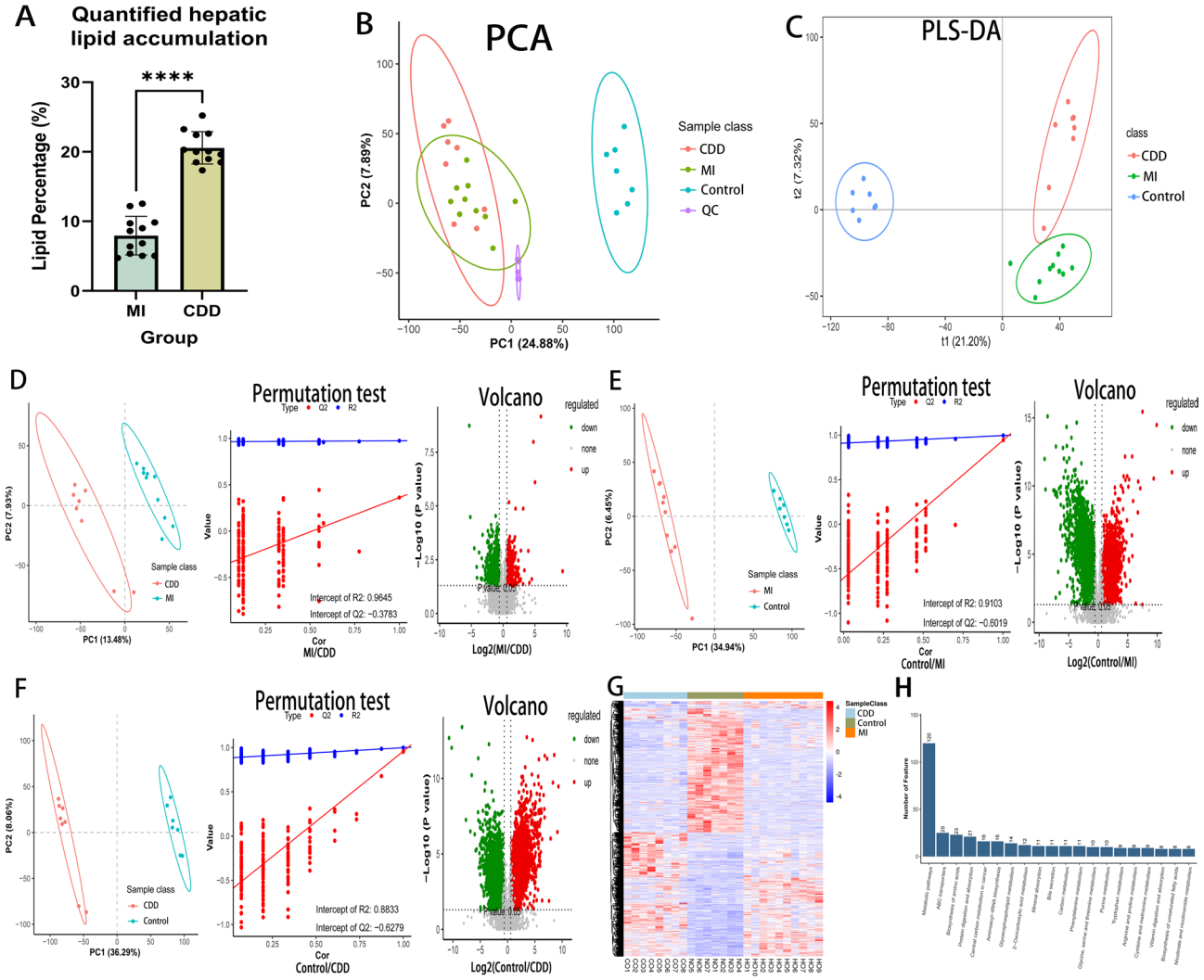

Fig. 5. Untargeted Metabolomics of Rat Liver. (**A**) Comparison of fat deposition in rat livers stained with Oil Red O between CDD and MI groups; (**B**) PCA analysis of metabolic ions from liver samples of all three rat groups and quality control samples; (**C**) PLS-DA analysis based on liver metabolites for comparison groups; (**D**) PLS-DA score plots for CDD and MI groups, permutation test plots based on PLS-DA, and volcano plots of metabolic changes; (**E**) PLS-DA score plots for MI and control groups, permutation test plots based on PLS-DA, and volcano plots of metabolic changes; (**F**) PLS-DA score plots for CDD and control groups, permutation test plots based on PLS-DA, and volcano plots of metabolic changes; (**G**) Heatmap displaying normalized detection intensities of metabolites after clustering of different samples; (**H**) Top 20 pathways involving secondary identified metabolites and their quantities. Con/Control: control group with standard diet; CDD: choline-deficient high-fat diet group; MI: metformin-treated choline-deficient high-fat diet group; p-values obtained via two-tailed unpaired Student's t-tests; $^{*}p < 0.05$; $^{**}p < 0.01$; $^{***}p < 0.001$; $^{****}p < 0.0001$; ns: no significance.

Comparison	pos_all	pos_up	pos_down	neg_all	neg_up	neg_down	all_regulate
MI/CDD	968	375	593	363	170	193	1331
Control/CDD	3151	1568	1583	2145	1227	918	5296
MI/Control	3210	1479	1731	2117	905	1212	5327

Table 1. Statistical comparison of metabolic ion differences among groups. Comparison: Comparative groups A/B, with B as the control; ALL: Total number of high-quality features used for quantification; Up: Number of features upregulated in sample A; Down: Number of features downregulated in sample A; pos: positive; neg: negative.

metabolites corresponding to each entry on the vertical axis. The illustration reveals that the pathways with the highest number of metabolites include 'metabolic pathways', 'ABC transporters', and the 'biosynthesis of amino acids'.

Figure 6A displays a heatmap showcasing the overall metabolic differences, normalized and categorized by groups and Fig. 7 presents a comparative analysis of metabolic ions between two groups, filtered based on Variable Importance in Projection (VIP) values and p-values ≤ 0.05. This is followed by standard normalization and logarithmic scaling (log10d), with annotations using MS2Metabolite. Figure 6B employs a bubble chart to demonstrate the enrichment levels of overall KEGG differential metabolites. Figures 6C-E depict comparative results of KEGG enrichment obtained from pairwise comparisons between groups. The Rich Factor denotes the number of differential metabolites in a given KEGG pathway divided by the total number of metabolites in that pathway, with smaller p-values indicating higher KEGG enrichment. Overall, metabolic changes appear to have a strong correlation with 'central carbon metabolism in cancer.' In terms of metabolic pathways, significant impacts are observed on the 'pentose phosphate pathway,' 'steroid hormone biosynthesis,' 'arachidonic acid metabolism,' 'linoleic acid metabolism,' and the biosynthesis of 'valine, leucine, and isoleucine.' Notable effects are also evident on the 'PPAR signaling pathway,' the 'intestinal immune network for IgA production,' and the 'serotonergic synapse.'

In the group comparisons, MAFLD rats exhibited enriched expression in the 'pentose phosphate pathway,' 'steroid hormone biosynthesis,' 'arachidonic acid metabolism,' and 'linoleic acid metabolism' relative to the control group rats. Post-treatment with metformin, MAFLD rats demonstrated lesser enrichment in 'endocrine resistance' compared to untreated MAFLD rats. In terms of lipid metabolism, the enrichment level of 'arachidonic acid metabolism' in the livers of drug-treated rats appeared surprisingly positive. Additionally, the enrichment in 'linoleic acid metabolism' and 'alpha-linolenic acid metabolism' was also superior in the treated MAFLD rats compared to the untreated ones. After drug treatment in MAFLD rats, there was a decrease in the enrichment of 'Retinol metabolism.' These pathway alterations may contribute to the reduced fat accumulation. Similarly, treated MAFLD rats displayed differences in enrichment levels in the 'PPAR signaling pathway,' the 'intestinal immune network for IgA production,' and the 'serotonergic synapse' compared to untreated rats. Specifically, the enrichment of the 'PPAR signaling pathway' decreased post-treatment, while the 'intestinal immune network for IgA production' and the 'serotonergic synapse' showed an increase.

The heatmap in Supplementary Fig. 8 highlights the clear metabolic differences between rats. The most notable changes include increased expression of 'Warfarin,' 'LysoPE 22:5,' 'Formiminoglutamic,' '2,5-Dimethoxy-4-isopropylthiophenethylamine,' and '4-hydroxy-2H-chromen-2-one,' along with decreased expression of '1-(beta-D-Ribofuranosyl)-1,4-dihydronicotinamide,' 'Daidzein,' 'Apigenin,' 'Enterolactone,' 'Glu-Leu,' 'Ethoxyquin,' and 'LysoPS 20:5'. Regarding the effects of metformin intervention, we focused on the treated MAFLD rats, where an evident increase in the expression of '1-(beta-D-Ribofuranosyl)-1,4-dihydronicotinamide,' 'DL-Norleucinamide,' and 'Nudifloramide' was observed, while expressions of 'D-Alloisoleucine,' '3-[3-(Sulfooxy)phenyl] propanoic acid,' '2-Methylbenzothiazole,' '4-Heptenal diethyl acetal,' '3alpha,7alpha,12alpha,25-Tetrahydroxy-5beta-cholestane-24-one,' and 'Thioarginine' decreased significantly. Therefore, leveraging the significant differences in metabolites between the two groups (VIP > 1 and $P < 0.05$), further analysis was conducted on related metabolic pathways (Supplementary Fig. 9). The data indicates that in MAFLD and liver fibrosis rats, the primary affected pathways were 'Pantothenate and CoA biosynthesis,' 'Glutathione metabolism,' and 'Purine metabolism.' Post-metformin treatment, 'Nicotinate and nicotinamide metabolism,' 'Pyrimidine metabolism,' 'Pentose phosphate pathway,' 'Glutathione metabolism,' and 'Histidine metabolism' in MAFLD rats were significantly impacted.

In summary, these results suggest substantial alterations in the metabolic patterns of MAFLD rats, with metformin playing a role in reversing these changes.

Lipid metabolism analysis

Supplementary Fig. 5 and Supplementary Table 2 presents the TIC and the distribution of metabolites in terms of m/z-retention time (rt) for lipidomic studies. Supplementary Fig. 6 and Table 2 illustrate the variations in lipid metabolism, with 29,799 positive metabolites and 26,656 negative metabolites identified within the lipid metabolism category of the HMDB Super class.

Figure 7A's KEGG pathway classification chart demonstrates that lipid metabolism and the metabolism of cofactors and vitamins have the highest number of metabolites. Figure 7B lists the top 40 pathway entries in the secondary identification of metabolite differences, highlighting the metabolic pathways in which 17 metabolites undergo changes. Table 2 and Supplementary Fig. 7 display the number of upregulated and downregulated metabolites between different groups. There are significant differences, amounting to thousands of metabolites, in the lipid metabolism between normal and MAFLD rats. However, the difference in lipid metabolism between metformin-treated and untreated MAFLD rats is smaller, with a total of 158 metabolic ions showing significant changes. PCA and PLS-DA score plots in Figs. 7C and D illustrate significant differences in lipid metabolites between MAFLD and control rats, and between medicated and unmedicated rats. Detailed comparisons between these groups are presented in Fig. 8.

The cluster analysis heatmap in Fig. 7E reveals distinct differences in lipid metabolites between groups, with the expression levels in the QC group indicating effective quality control. The chart clearly demonstrates significant disparities in lipid metabolism among the groups.

Figure 8 presents the PLS-DA score plots for pairwise comparisons among three groups, along with permutation tests and volcano plots for differential metabolites. The permutation plots reveal that all three comparison models exhibit no overfitting, as evidenced by all Q2 values being less than 0. This indicates that the models are robust and that the differences in metabolites between the groups are statistically significant, not merely a result of overfitting in the model.

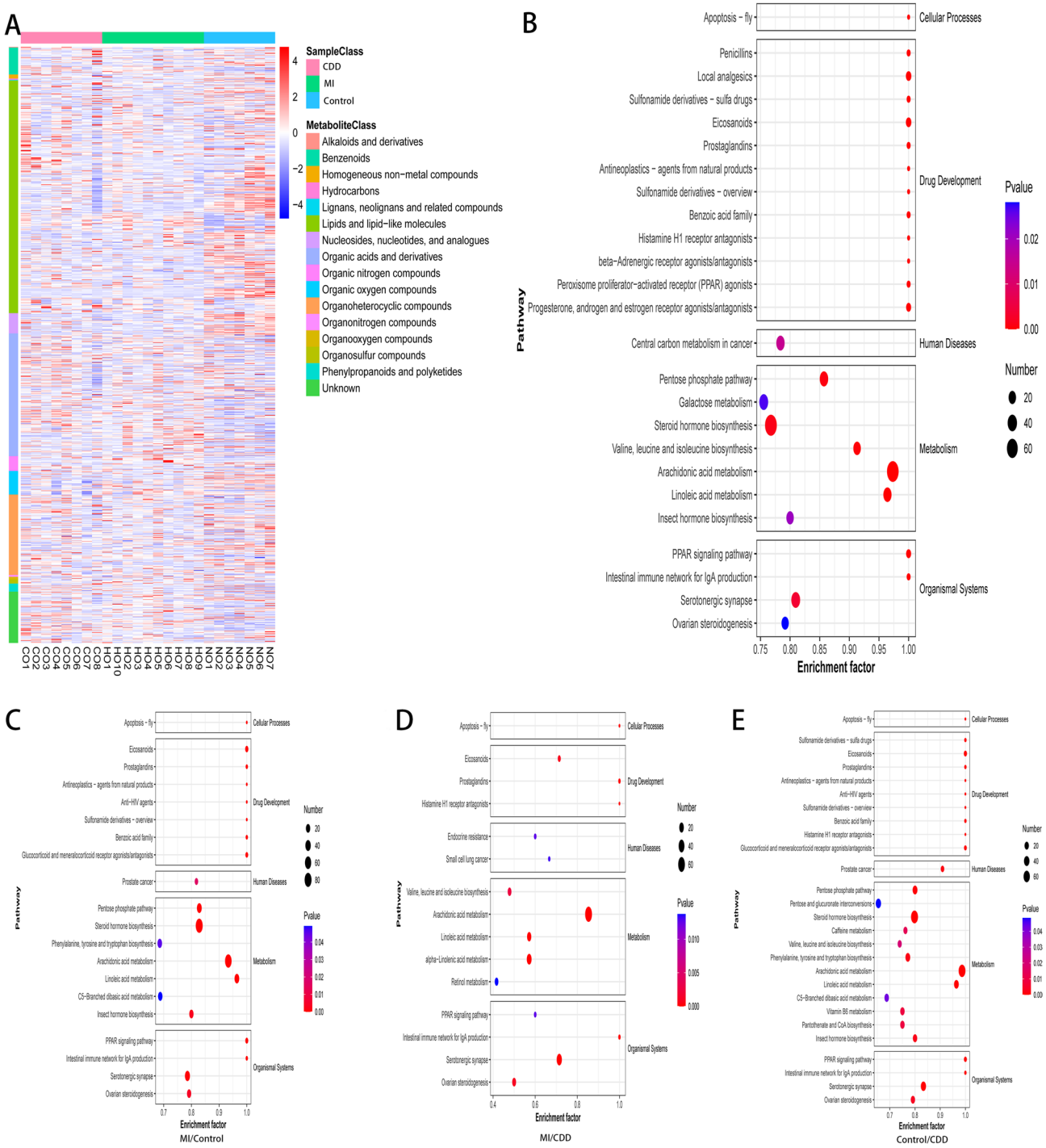

Fig. 6. Comparison of untargeted metabolomics in rat livers. (**A**) Overall metabolic differences normalized and categorized by groups. (**B**) Results of KEGG enrichment analysis represented by the Rich Factor (http://www.KEGG.jp/KEGG/kegg1.html), indicating the number of differential metabolites in a given KEGG pathway relative to the total number of metabolites in that pathway, visualized using ggplot2. (**C**) Differences in KEGG enrichment of differential metabolites between the MI group and the control group in rats. (**D**) Differences in KEGG enrichment of differential metabolites between the MI group and the CDD group in rats. (**E**) Differences in KEGG enrichment of differential metabolites between the CDD group and the control group in rats. Con/Control refers to the control group with a standard diet; CDD denotes the group with a choline-deficient, high-fat diet; MI indicates the group treated with metformin on a choline-deficient, high-fat diet. Kanehisa, M.; "Post-genome Informatics", Oxford University Press (2000).

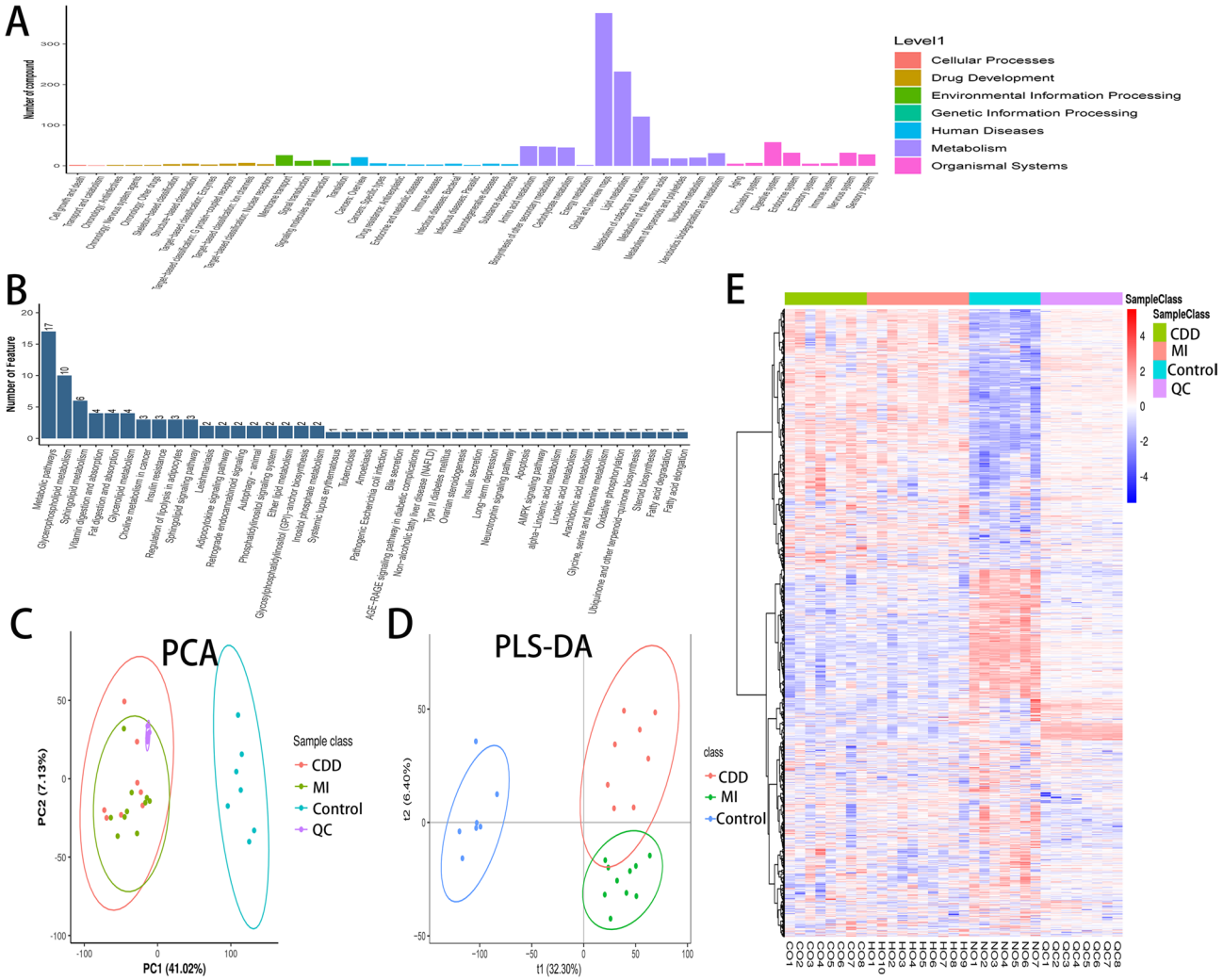

Fig. 7. Comparison of lipid metabolite differences in rat livers across groups. (**A**) KEGG pathway classification chart. (**B**) The top 40 pathway entries involving metabolites identified at the secondary level of metabolic differences. (**C**) PCA analysis of lipid metabolism ions from liver samples of all three groups of rats and quality control samples. (**D**) PLS-DA analysis based on liver lipid metabolites in the control group. (**E**) Grouped display of the detection intensity information of each metabolite in different samples (after normalization of intensity values). Con/Control refers to the control group with a standard diet; CDD denotes the group with a choline-deficient high-fat diet; MI indicates the group treated with metformin on a choline-deficient high-fat diet.

Comparison	pos_all	pos_up	pos_down	neg_all	neg_up	neg_down	all_regulate
MI/CDD	90	17	73	68	4	64	158
Control/CDD	2935	1110	1825	1651	601	1050	4586
MI/Control	2963	1813	1150	1460	973	487	4423

Table 2. Statistical comparison of lipid metabolic ion differences among Groups. Comparison: Comparative groups A/B, with B as the control; ALL: Total number of high-quality features used for quantification; Up: Number of features upregulated in sample A; Down: Number of features downregulated in sample A; pos: positive; neg: negative.

Supplementary Fig. 8A depicts a KEGG bubble chart for differential metabolites using ggplot2, illustrating the KEGG enrichment analysis results through a scatter plot. The Rich Factor represents the number of differential metabolites in a given KEGG pathway divided by the total number of metabolites in that pathway. It is evident from the chart that lipid metabolism plays a significant role in NAFLD and small-cell lung cancer. In terms of metabolic pathways, there are noticeable enrichments in 'Galactose metabolism,' 'Steroid

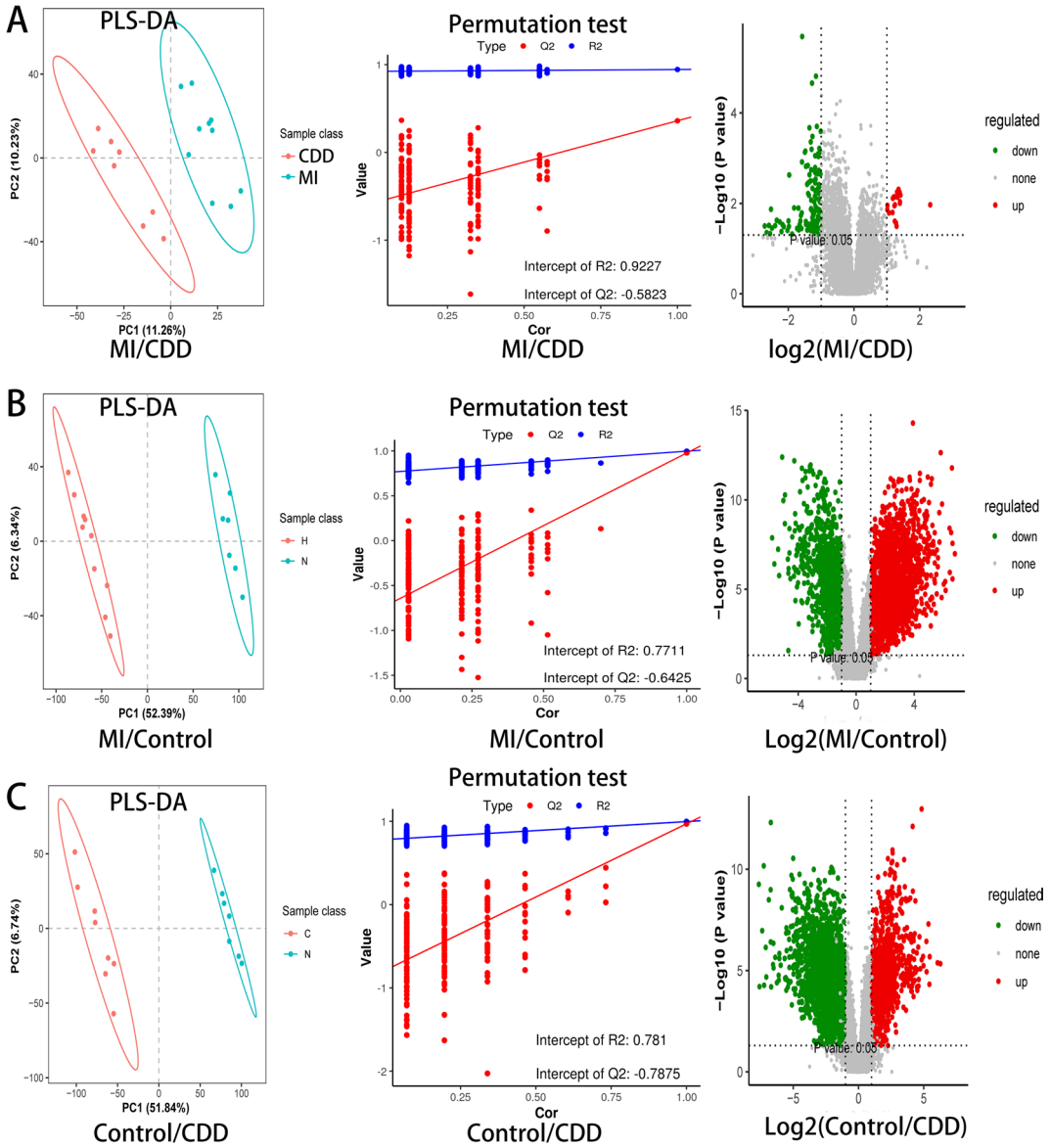

Fig. 8. Inter-group differences in lipid metabolites in rat livers. (A) PLS-DA score plots for the MI and CDD groups, including permutation test plots based on PLS-DA and volcano plots of metabolic changes. (B) PLS-DA score plots for the MI and control groups, featuring permutation test plots based on PLS-DA and volcano plots of metabolic changes. (C) PLS-DA score plots for the CDD and control groups, with permutation test plots based on PLS-DA and volcano plots of metabolic changes. Con/Control refers to the control group with a standard diet; CDD denotes the group with a choline-deficient, high-fat diet; MI indicates the group treated with metformin on a choline-deficient, high-fat diet.

biosynthesis,' 'Primary bile acid biosynthesis,' 'Arachidonic acid metabolism,' 'Linoleic acid metabolism,' and 'Retinol metabolism.' The 'PPAR signaling pathway,' 'Longevity regulating pathway-worm,' 'Intestinal immune network for IgA production,' 'Serotonergic synapse,' and 'Phototransduction-fly' also show changes. Notably, the unusual enrichment of 'Ovarian steroidogenesis' in all-male rats suggests a potential resistance to MAFLD progression, as estrogen inhibits abnormal fat deposition and appears to resist fibrosis. The group clustering analysis results (Supplementary Fig. 10B) reveal significant differences in lipid metabolism pathways between the three groups of rats, indicating changes in metabolic patterns among them. These changes are further compared in Supplementary Fig. 7.

Although the differences are not as pronounced as those between the MAFLD model and the normal rat model, there are still noticeable changes in the lipid metabolites of the rat liver after metformin treatment. Supplementary Fig. 10C-E display KEGG bubble charts depicting differential metabolites associated with hepatic lipid metabolism across three groups of rats. Relative to the control group, untreated MAFLD rats exhibited pronounced aberrant enrichment in pathways such as 'Galactose metabolism,' 'Steroid biosynthesis,' 'Primary bile acid biosynthesis,' 'Arachidonic acid metabolism,' 'Linoleic acid metabolism,' 'Alpha-linolenic acid metabolism,'

'Retinol metabolism,' and 'Biosynthesis of unsaturated fatty acids.' These alterations suggest a broad disruption of metabolic processes, encompassing carbohydrate metabolism, steroid biosynthesis, bile acid synthesis, and the metabolism of various fatty acids and vitamin A. In contrast, rats treated with metformin did not display this aberrant enrichment in 'Galactose metabolism' and 'Primary bile acid biosynthesis,' indicating that metformin may exert a regulatory effect on these specific metabolic pathways, potentially aiding in the restoration of normal metabolic function or at least mitigating metabolic dysregulation. Post-metformin treatment, MAFLD rats showed a marked reduction in the number of aberrant metabolites. Compared to untreated MAFLD counterparts, several lipid metabolism-related signaling pathways and functional networks were aberrantly enriched, including 'PPAR signaling pathway,' 'Vascular smooth muscle contraction,' 'Regulation of lipolysis in adipocytes,' 'Aldosterone synthesis and secretion,' 'Fat digestion and absorption,' and 'Vitamin digestion and absorption.' Notably, 'Regulation of lipolysis in adipocytes,' 'Fat digestion and absorption,' and 'Vitamin digestion and absorption' are closely linked to the processes of lipid metabolism and deposition, while 'Vascular smooth muscle contraction' and 'Aldosterone synthesis and secretion' may be related to the development of hepatic fibrosis. These pathways could be critical in the metformin-mediated delay of abnormal fat deposition and fibrosis in MAFLD. Our findings underscore the potential of metformin to decelerate the progression of MAFLD by modulating multiple mechanisms, including direct effects on lipid metabolic pathways and improvements in the digestion and absorption of fatty acids and vitamins.

It is noteworthy that rats treated with metformin displayed metabolic alterations in the 'Sphingolipid signaling pathway' when compared to untreated MAFLD rats, as shown in Supplementary Fig. 10C. The sphingolipid signaling pathway is implicated in the regulation of a multitude of cellular functions, including cell survival, proliferation, and apoptosis. These processes play a crucial role in the development of hepatic lipid accumulation. Metabolites of sphingolipid metabolism, such as ceramides, have been implicated in the accumulation of fat in the liver, with studies confirming that ceramides are involved in the promotion of fatty acid synthesis and storage.

Furthermore, disease-relevance analysis has confirmed an abnormal enrichment in conditions related to human NAFLD in MAFLD rats, regardless of metformin intervention, validating the accuracy of the model used in this study.

Quality evaluation of metabolomics data

In tissue metabolomics, the QC samples exhibiting good clustering in the PCA score plot indicate that the sample preprocessing and experimental conditions are reliable, ensuring the accuracy of the data obtained. This clustering demonstrates consistency and stability in the metabolic profiles across the QC samples, reflecting the robustness of the analytical method and the reliability of the subsequent results.

Discussion

MAFLD is a chronic liver condition characterized by fat accumulation in the liver, often associated with metabolic dysregulation, and is increasingly prevalent worldwide. Current research suggests a crucial role of gut microbiota dysbiosis in MAFLD, particularly in liver metabolism and inflammatory processes[33–35]. The gut microbiome, a complex ecosystem, interacts with the host to influence the health of various organs, including the liver[36,37]. In MAFLD, imbalances in gut microbiota may impair intestinal barrier functions, potentially increasing the entry of enterogenic toxins into the bloodstream, which can directly or indirectly affect liver metabolism and inflammation[38,39]. Furthermore, alterations in the gut microbiome are linked to liver lipid metabolism disorders. Changes in microbial composition, such as a decrease in Firmicutes and an increase in Bacteroidota, have been closely associated with dysregulated fat metabolism[40–42]. These alterations could contribute to the development of MAFLD. Conversely, an increase in bacteria like Shigella and Enterococcus in MAFLD patients may relate to liver inflammation and fibrosis[43,44]. Our study observed specific changes in the abundance of gut microbial groups in MAFLD rats, such as increased Alistipes, Desulfovibrionaceae, Tyzzerella, and Peptococcaceae, and a significant decrease in Akkermansia, Ligilactobacillus, and Lactobacillus. Additionally, major phyla such as Firmicutes, Bacteroidota, and Verrucomicrobiota showed relative abundance variations across different groups.

Dietary choline deprivation serves as a classical experimental model for studying the pathophysiology of MAFLD. Its central mechanism lies in disrupting hepatic phosphatidylcholine (PC) synthesis and very-low-density lipoprotein (VLDL) secretion. Under choline-deficient dietary conditions, insufficient methyl donors impair hepatic PC synthesis, leading to defective lipid assembly into VLDL particles and their subsequent secretion into the bloodstream. This blockade triggers abnormal intracellular triglyceride (TG) accumulation, directly driving steatosis. Notably, the choline deprivation model not only recapitulates the fatty liver phenotype in rodents but also demonstrates high pathophysiological relevance to human lean MAFLD, as it bypasses confounding metabolic factors like obesity and insulin resistance. This underscores the conserved role of the PC/VLDL pathway as a core mechanism for hepatocyte lipid export across species. Recent studies further reveal that prolonged choline deprivation activates hepatic stellate cells, driving collagen deposition and fibrotic progression via oxidative stress and mitochondrial dysfunction (like CPT1A-mediated inhibition of fatty acid oxidation), thereby establishing a pathological cascade from simple steatosis to steatohepatitis and fibrosis. This choline-deficient model provides a unique tool for dissecting obesity-independent drivers of lean MAFLD, particularly in metabolic disturbances dominated by mitochondrial lipid dysmetabolism or ER stress-related lipotoxicity. Its translational value lies in identifying impaired PC synthesis and VLDL secretion defects as potential therapeutic targets for lean MAFLD patients, while offering a standardized platform for screening weight-loss-independent therapeutic strategies targeting these pathways.

The results demonstrate that metformin significantly alters the abundance of specific microorganisms, with certain microbial populations showing a marked decrease, while others increase, indicating a profound impact of metformin on the gut microbiome. Notably, after the administration of metformin, there was a

significant reduction in the relative abundance of microorganisms such as '*g__Desulfovibrionaceae_unclassified*', '*g__Alloprevotella*', '*g_Bilophila*', '*g_Blautia*', 'g_Romboutsia', and '*g_Rhodococcus*', while '*g_Eubacterium_coprostanoligenes_group*', '*g__Prevotellaceae_UCG_001*', and '*g_Parabacteroides*' saw a considerable increase. This underscores the significant influence of metformin on the composition and dynamics of the intestinal microbiota. The alterations in these microbial communities indicate the inhibitory effect of metformin on chronic inflammatory responses caused by MAFLD[45]. At the same time, the changes in the microbial communities assist in converting cholesterol within the body into coprostanol, a form less readily absorbed[46,47]. This process potentially aids in reducing cholesterol levels in the blood, subsequently influencing the deposition of lipids in the liver.

Furthermore, an analysis of hepatic metabolites in MAFLD rats revealed that over a thousand changes occurred under the influence of metformin, involving 56,471 identified metabolites, including lipids, organic oxygen compounds, and organic acids. These alterations are associated with aspects such as the onset and progression of human tumors, as well as digestive and endocrine systems. Significant differences in metabolic patterns were confirmed among the control, MAFLD, and metformin-treated groups. Overall, these findings, as shown in Supplementary Fig. 11, highlight the dual impact of metformin on the gut microbiota and liver metabolism in rats, particularly its prominent role in the regulation of lipid metabolism. This provides crucial insights for further research into the potential mechanisms of metformin in the treatment of metabolic diseases.

Dysbiosis of the gut microbiome, or an imbalance in the intestinal microbial community, and alterations in liver metabolism play crucial roles in the pathogenesis of MAFLD. The gut microbiota interacts with the host's metabolism through various mechanisms. Specifically, in the MAFLD rat model, dysbiosis of the gut microbiota can lead to impaired intestinal barrier function[48–50]. This impairment increases the translocation of endotoxins and other inflammatory inducers, which, via the portal vein, enter the liver and cause local alterations in hepatic metabolic patterns. Additionally, the gut microbiome is capable of regulating bile acid metabolism, thereby influencing hepatic lipid metabolism and energy balance[51–53]. The liver, as the center of metabolic activity, is responsible for the synthesis and breakdown of lipids. In the realm of liver lipid metabolism, research has uncovered that butyrate treatment reduces triglyceride accumulation and impacts the expression of genes associated with lipid and glucose metabolism[54–56]. Furthermore, butyrate enhances the clearance and oxidation of fatty acids, and influences the expression of genes linked to inflammation and tissue remodeling[57,58]. These findings highlight the crucial role of butyrate and its producing bacteria in liver lipid metabolism, suggesting their potential in alleviating MAFLD.

In the pathological analysis of liver tissue sections, we found that metformin plays a certain role in delaying liver fibrosis. Pathological results indicate that, although the metformin group also exhibited a tendency towards liver fibrosis, the degree of liver damage and the severity of fibrosis were lower compared to the HFD group. Therefore, we can deduce that metformin possesses the capacity to maintain normal liver function and slow down the progression of fibrosis. Recent studies have increasingly focused on the potential therapeutic role of metformin in liver fibrosis[59–61]. Metformin has shown promise in modulating pathways associated with hepatic fibrosis. Its mechanism of action is multifaceted, involving the activation of AMPK, a crucial regulator of cellular energy homeostasis[62–64]. Activation of AMPK by metformin leads to the inhibition of hepatic stellate cells (HSCs), the key effector cells in the development of liver fibrosis[65,66]. Additionally, metformin exerts anti-inflammatory and anti-oxidative effects, which are beneficial in alleviating chronic liver inflammation and oxidative stress, thereby potentially impeding the progression of fibrosis[67]. These studies suggest that metformin's potential role extends beyond glucose regulation, indicating its capability to attenuate liver fibrosis through the modulation of lipid metabolism and cellular stress responses. However, further research is needed to fully understand metformin's therapeutic mechanisms. Before definitive clinical evidence and safety assessments are established, the use of this drug should be approached with caution.

The interaction between the gut microbiome and liver metabolism forms what is known as the "gut-liver axis," which plays a central role in the development of MAFLD[68]. Dysbiosis in the gut microbiota, leading to an increase in endotoxins and the production of inflammatory mediators, can directly impact liver metabolism, exacerbating liver cell damage and fibrosis. At the same time, changes in liver metabolism can reciprocally affect the composition and function of the gut microbiota. Therefore, research on the gut-liver axis in MAFLD patients is not only necessary but also holds potential for clinical translation. It is noteworthy that in MAFLD rats, there is a significant increase in the presence of the *Desulfobacterota* phylum, which is not observed in the intestines of normal rats. Research has confirmed that changes in the *Desulfobacterota* phylum are associated with certain disease states, such as MAFLD, inflammatory bowel disease, and colorectal cancer[69,70]. In these diseases, an abnormal increase in *Desulfobacterota* may be related to the onset and progression of the disease. Our study findings further corroborate the correlation between this type of microorganism and MAFLD.

In MAFLD rats undergoing metformin treatment, significant changes were observed in the gut microbial community, particularly a notable decline in specific microbial categories compared to untreated MAFLD rats. These include the Alistipes genus, Firmicutes phylum, Tannerellaceae family, and Ruminococcus genus. These alterations suggest that metformin may exert its therapeutic effects by modifying the composition of gut microbiota, impacting the abundance and diversity of these microbial communities. Such shifts in the microbiome could be related to metformin's role in regulating metabolism, enhancing insulin sensitivity, and other potential health benefits. This discovery provides crucial insights into understanding the mechanisms of action of metformin and the complex interactions between gut microbiota and host health.

After treatment with metformin, significant alterations were observed in the metabolic aspects of MAFLD rats. There was a heightened enrichment in lipid metabolism pathways like "arachidonic acid metabolism," "linoleic acid metabolism," and "alpha-linolenic acid metabolism," while there was a reduction in the enrichment of "retinol metabolism," potentially linked to decreased fat accumulation. In signaling pathways, post-treatment showed a decrease in the enrichment of the "PPAR signaling pathway," but an increase in the "intestinal immune

network for IgA production" and the "serotonergic synapse." Moreover, changes were noticed in the expression of specific metabolites; "1-(beta-D-Ribofuranosyl)-1,4-dihydronicotinamide," "DL-Norleucinamide," and "Nudifloramide" saw an increase, whereas "D-Alloisoleucine" and "Thioarginine" experienced a significant decrease. The treatment with metformin also profoundly impacted "nicotinate and nicotinamide metabolism," "pyrimidine metabolism," "pentose phosphate pathway," "glutathione metabolism," and "histidine metabolism." These findings indicate that metformin's effects extend beyond specific metabolic pathways, influencing lipid metabolism, signaling processes, and mechanisms related to intestinal immunity and neuro-transmission. Currently, the role of metformin in regulating lipid metabolism disorders has also garnered interest among researchers. In mouse experiments, metformin has been proven to effectively reduce metabolic disorders and kidney damage caused by a high-fat diet[71]. It lowers the expression of fat-induced factors, reduces macrophage infiltration, and decreases triglyceride levels in the liver. Combined use of metformin with pioglitazone significantly reduces elevated levels of free fatty acids (FFA), diacylglycerol, and triglycerides[72]. It also diminishes the expression of genes associated with FFA uptake and de novo lipogenesis, including Cd36, Fads1, Fads2, and Pklr[73].

Lipid metabolism, along with cofactor and vitamin metabolism, plays a significant role in NAFLD. Notably, significant abnormalities are observed in pathways such as 'galactose metabolism,' 'steroid biosynthesis,' and 'bile acid biosynthesis.' Post-treatment with metformin, MAFLD rats demonstrated notable changes in certain metabolic pathways, particularly in 'PPAR signaling' and 'fat digestion and absorption.' This suggests that metformin may regulate these specific metabolic pathways, aiding in restoring normal metabolic functions or at least alleviating metabolic dysregulation. Compared to untreated MAFLD rats, those treated with metformin exhibited metabolic changes in the 'phosphatidylinositol signaling pathway', which plays a critical role in regulating various cellular functions, including cell survival, proliferation, and apoptosis, and is crucial for the development of hepatic fat accumulation[74]. After metformin treatment, MAFLD rats showed a relative decrease in the enrichment of 'endocrine resistance.' In terms of lipid metabolism, there was an unexpected positive change in the enrichment of 'arachidonic acid metabolism' in the livers of the treated rats. Furthermore, 'linoleic acid metabolism' and 'alpha-linolenic acid metabolism' were also superior in the treated MAFLD rats compared to the untreated ones. Post-treatment, there was a decrease in the enrichment of 'retinol metabolism' in MAFLD rats, suggesting a potential link between metformin and the activation of HSCs. Notably, metformin treatment showed significant regulatory effects on certain pathways, such as 'regulation of lipolysis in adipocytes,' 'fat digestion and absorption,' and 'vitamin digestion and absorption,' which are closely related to the process of lipid metabolism and deposition. Pathways like 'vascular smooth muscle contraction' and 'aldosterone synthesis and secretion' may be linked to the development of liver fibrosis. These pathways could be key to metformin's role in delaying abnormal fat deposition and fibrosis in MAFLD.

The choline-deficient, high-fat diet model in rodents, while valuable for studying hepatic VLDL synthesis defects and steatosis progression, exhibits some divergences from human lean MAFLD pathophysiology that warrant caution in translational interpretations. A key distinction lies in the accelerated fibrosis timeline in rodent models, where advanced collagen deposition can occur within weeks of dietary intervention, contrasting sharply with the years-long, multifactorial fibrotic progression observed in humans. This discrepancy arises from the absence of human-relevant genetic and environmental variabilities in controlled rodent settings—such as polygenic risk factors, microbiome diversity, or lifestyle heterogeneity—which collectively modulate disease severity and therapeutic responses in human populations. Furthermore, the rat model bypasses obesity-independent but clinically relevant drivers of lean MAFLD (such as mitochondrial dysfunction, hormonal influences, or epigenetic modifications) by mechanistically overemphasizing acute lipid-export blockade. These artificial constraints limit the model's capacity to replicate the stochasticity of human disease, particularly in non-obese individuals with heterogeneous metabolic etiologies. Importantly, environmental factors like chronic low-grade endotoxemia, circadian disruption, or intermittent nutrient stressors—common in human MAFLD—are absent in standardized rodent protocols. Researchers must explicitly avoid overgeneralizing findings from such accelerated, reductionist models to all MAFLD subtypes without rigorous validation in human cohorts. To bridge these translational gaps, future studies should prioritize human microbiota-transplanted gnotobiotic models to recapitulate host-microbe crosstalk, coupled with longitudinal dietary interventions mimicking real-world metabolic variability. This approach would better align preclinical data with the complex, multifactorial nature of lean MAFLD while preserving the mechanistic insights provided by the rat model.

In summary, our study has confirmed changes in the gut microbiome and liver metabolic patterns during the liver fibrosis process in lean MAFLD rats. The use of metformin can, to some extent, slow the progression of liver fibrosis by influencing both gut microbiota and hepatic metabolic patterns.

Data availability

The raw sequence data reported in this paper have been deposited in the Genome Sequence Archive (Genomics, Proteomics & Bioinformatics 2021) in National Genomics Data Center (Nucleic Acids Res 2022), China National Center for Bioinformation / Beijing Institute of Genomics, Chinese Academy of Sciences (GSA: CRA014724) that are publicly accessible at https://ngdc.cncb.ac.cn/gsa[75,76]. We show our full respect and gratitude to all the participants in the study. The mechanism illustrations were created by Figdraw (http://www.figdraw.com).The datasets used and/or analyzed during the current study are available from the corresponding author on reasonable request.

Received: 20 January 2025; Accepted: 16 June 2025
Published online: 02 July 2025

References

1. Eslam, M. et al. A new definition for metabolic dysfunction-associated fatty liver disease: an international expert consensus statement. *J. Hepatol.* **73**(1), 202–209. https://doi.org/10.1016/j.jhep.2020.03.039 (2020).
2. Shiha, G. et al. Redefining fatty liver disease: an international patient perspective. *Lancet Gastroenterol. Hepatol.* **6**(1), 73–79. https://doi.org/10.1016/s2468-1253(20)30294-6 (2021).
3. Bellentani, S. The epidemiology of non-alcoholic fatty liver disease. *Liver Int. Off. J. Int. Assoc. Study Liver*. 81–84. https://doi.org/10.1111/liv.13299 (2017).
4. Zeybel, M. et al. Multiomics analysis reveals the impact of microbiota on host metabolism in hepatic steatosis. *Adv. Sci.* **9**(11), e2104373. https://doi.org/10.1002/advs.202104373 (2022).
5. Estes, C. et al. Modeling the epidemic of nonalcoholic fatty liver disease demonstrates an exponential increase in burden of disease. *Hepatol. (Baltimore Md)*. **67**(1), 123–133. https://doi.org/10.1002/hep.29466 (2018).
6. Cespiati, A. et al. An overview of hepatocellular carcinoma surveillance focusing on non-cirrhotic NAFLD patients: A challenge for physicians. *Biomedicines* **11**(2). https://doi.org/10.3390/biomedicines11020586 (2023).
7. Li, H. et al. Prevalence and risk factors of metabolic associated fatty liver disease in xinxiang, China. *Int. J. Environ. Res. Public Health*. **17**(6). https://doi.org/10.3390/ijerph17061818 (2020).
8. Younossi, Z. et al. The global epidemiology of NAFLD and NASH in patients with type 2 diabetes: A systematic review and meta-analysis. *J. Hepatol.* **71**(4), 793–801. https://doi.org/10.1016/j.jhep.2019.06.021 (2019).
9. Lu, Y. et al. Chinese visceral adipose index shows superior diagnostic performance in predicting the risk of metabolic dysfunction associated fatty liver disease in early postmenopausal Chinese women. *Diabetes Metab. Syndr. Obes. Targets Ther.* **16**, 607–617. https://doi.org/10.2147/dmso.S402814 (2023).
10. Fabbrini, E., Sullivan, S. & Klein, S. Obesity and nonalcoholic fatty liver disease: biochemical, metabolic, and clinical implications. *Hepatol. (Baltimore Md)*. **51**(2), 679–689. https://doi.org/10.1002/hep.23280 (2010).
11. Petersen, M. & Shulman, G. Mechanisms of insulin action and insulin Resistance. *Physiol. Rev.* **98**(4), 2133–2223. https://doi.org/10.1152/physrev.00063.2017 (2018).
12. Godoy-Matos, A., Silva Júnior, W. & Valerio, C. NAFLD as a continuum: from obesity to metabolic syndrome and diabetes. *Diabetol. Metab. Syndr.* **12**(60). https://doi.org/10.1186/s13098-020-00570-y (2020).
13. Rinella, M. et al. A multisociety Delphi consensus statement on new fatty liver disease nomenclature. *J. Hepatol.* **79**(6), 1542–1556. https://doi.org/10.1016/j.jhep.2023.06.003 (2023).
14. Parisinos, C. et al. Genome-wide and Mendelian randomisation studies of liver MRI yield insights into the pathogenesis of steatohepatitis. *J. Hepatol.* **73**(2), 241–251. https://doi.org/10.1016/j.jhep.2020.03.032 (2020).
15. Shao, C. et al. Metabolomics to identify fingerprints of carotid atherosclerosis in Nonobese metabolic dysfunction-associated fatty liver disease. *J. Translational Med.* **21**(1), 12. https://doi.org/10.1186/s12967-022-03760-6 (2023).
16. Heeren, J. & Scheja, L. Metabolic-associated fatty liver disease and lipoprotein metabolism. *Mol. Metabolism*. **50**, 101238. https://doi.org/10.1016/j.molmet.2021.101238 (2021).
17. Badmus, O. et al. Molecular mechanisms of metabolic associated fatty liver disease (MAFLD): functional analysis of lipid metabolism pathways. *Clin. Sci.* **136**(18), 1347–1366. https://doi.org/10.1042/cs20220572 (2022).
18. Rao, Y. et al. Gut Akkermansia muciniphila ameliorates metabolic dysfunction-associated fatty liver disease by regulating the metabolism of L-aspartate via gut-liver axis. *Gut Microbes*. **13**(1), 1–19. https://doi.org/10.1080/19490976.2021.1927633 (2021).
19. Yang, W. et al. Dorzagliatin add-on therapy to Metformin in patients with type 2 diabetes: a randomized, double-blind, placebo-controlled phase 3 trial. *Nat. Med.* **28**(5), 974–981. https://doi.org/10.1038/s41591-022-01803-5 (2022).
20. Griffith, R. et al. Interventions to prevent women from developing gestational diabetes mellitus: an overview of Cochrane Reviews. *Cochrane Database Syst. Rev.* **6**(6), CD012394. https://doi.org/10.1002/14651858.CD012394.pub3 (2020).
21. He, L. Metformin and systemic metabolism. *Trends Pharmacol. Sci.* **41**(11), 868–881. https://doi.org/10.1016/j.tips.2020.09.001 (2020).
22. Nicholson, G. & Hall, G. Diabetes mellitus: new drugs for a new epidemic. *Br. J. Anaesth.* **107**(1), 65–73. https://doi.org/10.1093/bja/aer120 (2011).
23. Kita, Y. et al. Metformin prevents and reverses inflammation in a non-diabetic mouse model of nonalcoholic steatohepatitis. *PloS One*. **7**(9), e43056. https://doi.org/10.1371/journal.pone.0043056 (2012).
24. Huang, Y. et al. Effect of Metformin on nonalcoholic fatty liver based on meta-analysis and network pharmacology. *Medicine* **101**(43), e31437. https://doi.org/10.1097/md.0000000000031437 (2022).
25. Han, Y. et al. Post-translational regulation of lipogenesis via AMPK-dependent phosphorylation of insulin-induced gene. *Nat. Commun.* **10**(1), 623. https://doi.org/10.1038/s41467-019-08585-4 (2019).
26. Li, S. et al. Metformin inhibits intracranial aneurysm formation and progression by regulating vascular smooth muscle cell phenotype switching via the AMPK/ACC pathway. *J. Neuroinflamm.* **17**(1), 191. https://doi.org/10.1186/s12974-020-01868-4 (2020).
27. Chen, K. et al. Advancing the understanding of NAFLD to hepatocellular carcinoma development: from experimental models to humans. *Biochim. Et Biophys. Acta Reviews cancer*. **1871**(1), 117–125. https://doi.org/10.1016/j.bbcan.2018.11.005 (2019).
28. Nevzorova, Y. et al. Animal models for liver disease - A practical approach for translational research. *J. Hepatol.* **73**(2), 423–440. https://doi.org/10.1016/j.jhep.2020.04.011 (2020).
29. Kanehisa, M., Symposium, N. F. & Kanehisa, M. The KEGG Database. *Novartis Found Symp.* **28**(1), 27–30 https://doi.org/10.1093/nar/28.1.27 (2002).
30. Kanehisa, M. & Goto, S. KEGG: Kyoto encyclopedia of genes and genomes. *Nucleic Acids Res.*, **27**(1), 29–34 https://doi.org/10.1093/nar/28.1.27 (1999).
31. Minoru, K. Toward Understanding the origin and evolution of cellular organisms. *Protein Sci.* **28**(11), 1947–1951. https://doi.org/10.1002/pro.3715 (2019).
32. Minoru, K. et al. KEGG for taxonomy-based analysis of pathways and genomes. *Nucleic Acids Res.* **51**(0). https://doi.org/10.1093/nar/gkac963 (2022).
33. Wang, W. et al. Ochratoxin A induces liver inflammation: involvement of intestinal microbiota. *Microbiome* **7**(1), 151. https://doi.org/10.1186/s40168-019-0761-z (2019).
34. Kirpich, I., Marsano, L. & McClain, C. Gut-liver axis, nutrition, and non-alcoholic fatty liver disease. *Clin. Biochem.* **48**, 923–930. https://doi.org/10.1016/j.clinbiochem.2015.06.023 (2015).
35. Rao, Y. et al. Bouchardatine analogue alleviates non-alcoholic hepatic fatty liver disease/non-alcoholic steatohepatitis in high-fat fed mice by inhibiting ATP synthase activity. *Br. J. Pharmacol.* **176**(16), 2877–2893. https://doi.org/10.1111/bph.14713 (2019).
36. Visconti, A. et al. Interplay between the human gut microbiome and host metabolism. *Nat. Commun.* **10**(1), 4505. https://doi.org/10.1038/s41467-019-12476-z (2019).
37. Hooper, L., Littman, D. & Macpherson, A. Interactions between the microbiota and the immune system. *Sci. (New York NY)*. **336**(6086), 1268–1273. https://doi.org/10.1126/science.1223490 (2012).
38. Mu, Q. et al. Pregnancy and lactation interfere with the response of autoimmunity to modulation of gut microbiota. *Microbiome* **7**(1), 105. https://doi.org/10.1186/s40168-019-0720-8 (2019).
39. Ma, L. et al. Spermidine improves gut barrier integrity and gut microbiota function in diet-induced obese mice. *Gut Microbes*. **12**(1), 1–19. https://doi.org/10.1080/19490976.2020.1832857 (2020).

40. Gagné, M. et al. Dysbiotic microbiota contributes to the extent of acute myocardial infarction in rats. *Sci. Rep.* **12**(1), 16517. https://doi.org/10.1038/s41598-022-20826-z (2022).
41. Li, N. et al. Cichorium intybusintegration of network Pharmacology and intestinal flora to investigate the mechanism of action of Chinese herbal formula in attenuating adenine and ethambutol hydrochloride-induced hyperuricemic nephropathy in rats. *Pharm. Biol.* **60**(1), 2338–2354. https://doi.org/10.1080/13880209.2022.2147551 (2022).
42. Jaimes, J. et al. Stool metabolome-microbiota evaluation among children and adolescents with obesity, overweight, and normal-weight using 1H NMR and 16S rRNA gene profiling. *PloS One*. **16**(3), e0247378. https://doi.org/10.1371/journal.pone.0247378 (2021).
43. Yin, H. et al. Fusobacterium nucleatum promotes liver metastasis in colorectal cancer by regulating the hepatic immune niche and altering gut microbiota. *Aging* **14**(4), 1941–1958. https://doi.org/10.18632/aging.203914 (2022).
44. Ermolenko, E. et al. Consortium of indigenous fecal bacteria in the treatment of metabolic syndrome. *Microorganisms* **10**(8). https://doi.org/10.3390/microorganisms10081574 (2022).
45. Wang, J. et al. Beneficial effects of ginger on prevention of obesity through modulation of gut microbiota in mice. *Eur. J. Nutr.* **59**(2), 699–718. https://doi.org/10.1007/s00394-019-01938-1 (2020).
46. Paramsothy, S. et al. Specific bacteria and metabolites associated with response to fecal microbiota transplantation in patients with ulcerative Colitis. *Gastroenterology* **156**(5), 1440–1454e1442. https://doi.org/10.1053/j.gastro.2018.12.001 (2019).
47. Srikanth, E. S. & Shreyas, M. Recent advances, novel targets and treatments for cholelithiasis; a narrative review. *Eur. J. Pharmacol.* **908**, 174376 https://doi.org/10.1016/j.ejphar.2021.174376 (2021).
48. Zhang, R. et al. Elevated serum levels of diamine oxidase, D-lactate and lipopolysaccharides are associated with metabolic-associated fatty liver disease. *Eur. J. Gastroenterol. Hepatol.* **35**(1), 94–101. https://doi.org/10.1097/meg.0000000000002456 (2023).
49. Jia, Q. et al. Fecal microbiota of diarrhea-predominant irritable bowel syndrome patients causes hepatic inflammation of germ-free rats and Berberine reverses it partially. *BioMed Res. Int.* **2019**, 4530203 https://doi.org/10.1155/2019/4530203 (2019).
50. Fuke, N. et al. Regulation of gut microbiota and metabolic endotoxemia with dietary factors. *Nutrients* **11**(10). https://doi.org/10.3390/nu11102277 (2019).
51. Liu, F. et al. Age-related alterations in metabolome and microbiome provide insights in dietary transition in giant pandas. *mSystems* **8**(3), e0025223. https://doi.org/10.1128/msystems.00252-23 (2023).
52. Culpepper, T. et al. Three probiotic strains exert different effects on plasma bile acid profiles in healthy obese adults: randomised, double-blind placebo-controlled crossover study. *Beneficial Microbes*. **10**(5), 497–509. https://doi.org/10.3920/bm2018.0151 (2019).
53. Fuchs, C. et al. Absence of Bsep/Abcb11 attenuates MCD diet-induced hepatic steatosis but aggravates inflammation in mice. *Liver International: Official J. Int. Association Study Liver*. **40**(6), 1366–1377. https://doi.org/10.1111/liv.14423 (2020).
54. Prins, G. et al. The effects of butyrate on induced metabolic-associated fatty liver disease in precision-cut liver slices. *Nutrients*. **13**(12). https://doi.org/10.3390/nu13124203 (2021).
55. Shen, T. et al. Sitagliptin reduces insulin resistance and improves rat liver steatosis via the SIRT1/AMPKα pathway. *Experimental Therapeutic Med.* **16**(4), 3121–3128. https://doi.org/10.3892/etm.2018.6554 (2018).
56. Ye, J. et al. Butyrate protects mice against methionine-choline-deficient diet-induced non-alcoholic steatohepatitis by improving gut barrier function, attenuating inflammation and reducing endotoxin levels. *Front. Microbiol.* **9**, 1967. https://doi.org/10.3389/fmicb.2018.01967 (2018).
57. Rose, S. et al. Butyrate enhances mitochondrial function during oxidative stress in cell lines from boys with autism. *Translational Psychiatry*. **8**(1), 42. https://doi.org/10.1038/s41398-017-0089-z (2018).
58. Li, H. et al. Sodium butyrate stimulates expression of fibroblast growth factor 21 in liver by Inhibition of histone deacetylase 3. *Diabetes* **61**(4), 797–806. https://doi.org/10.2337/db11-0846 (2012).
59. Zhang, A. et al. Research progress of metformin in the treatment of liver fibrosis. *Int. Immunopharmacol.* **116**, 109738. https://doi.org/10.1016/j.intimp.2023.109738 (2023).
60. Katsura, A. et al. MicroRNA profiles following Metformin treatment in a mouse model of non-alcoholic steatohepatitis. *Int. J. Mol. Med.* **35**(4), 877–884. https://doi.org/10.3892/ijmm.2015.2092 (2015).
61. Yang, X. et al. Predictive and preventive significance of AMPK activation on hepatocarcinogenesis in patients with liver cirrhosis. *Cell Death Dis.* **9**(3), 264. https://doi.org/10.1038/s41419-018-0308-4 (2018).
62. Qiao, Y. et al. Single cell derived spheres of umbilical cord mesenchymal stem cells enhance cell stemness properties, survival ability and therapeutic potential on liver failure. *Biomaterials* **227**, 119573. https://doi.org/10.1016/j.biomaterials.2019.119573 (2020).
63. Xu, X. et al. Nuclear UHRF1 is a gate-keeper of cellular AMPK activity and function. *Cell Res.* **32**(1), 54–71. https://doi.org/10.1038/s41422-021-00565-y (2022).
64. He, D. et al. A novel LncRNA MDHDH suppresses glioblastoma multiforme by acting as a scaffold for MDH2 and PSMA1 to regulate NAD + metabolism and autophagy. *J. Experimental Clin. cancer Research: CR*. **41**(1), 349. https://doi.org/10.1186/s13046-022-02543-7 (2022).
65. Alsamman, S. et al. Targeting acid ceramidase inhibits YAP/TAZ signaling to reduce fibrosis in mice. *Sci. Transl. Med.* **12**, 557. https://doi.org/10.1126/scitranslmed.aay8798 (2020).
66. Zhang, W. et al. Inactivation of NF-κB2 (p52) restrains hepatic glucagon response via preserving PDE4B induction. *Nat. Commun.* **10**(1), 4303. https://doi.org/10.1038/s41467-019-12351-x (2019).
67. Liu, H. et al. Metformin suppresses calcium oxalate crystal-induced kidney injury by promoting Sirt1 and M2 macrophage-mediated anti-inflammatory activation. *Signal. Transduct. Target. Therapy*. **8**(1), 38. https://doi.org/10.1038/s41392-022-01232-3 (2023).
68. Albillos, A., de Gottardi, A. & Rescigno, M. The gut-liver axis in liver disease: pathophysiological basis for therapy. *J. Hepatol.* **72**(3), 558–577. https://doi.org/10.1016/j.jhep.2019.10.003 (2020).
69. Liu, N. et al. Auricularia auriculaeffects of polysaccharides on gut microbiota composition in type 2 diabetic mice. *Molecules*. **27**(18). https://doi.org/10.3390/molecules27186061 (2022).
70. Goldstein, E. et al. Desulfovibrio desulfuricans bacteremia and review of human Desulfovibrio infections. *J. Clin. Microbiol.* **41**(6), 2752–2754. https://doi.org/10.1128/jcm.41.6.2752-2754.2003 (2003).
71. Kim, D. et al. Metformin decreases high-fat diet-induced renal injury by regulating the expression of adipokines and the renal AMP-activated protein kinase/acetyl-CoA carboxylase pathway in mice. *Int. J. Mol. Med.* **32**(6), 1293–1302. https://doi.org/10.3892/ijmm.2013.1508 (2013).
72. Bailey, C. Treating insulin resistance in type 2 diabetes with metformin and thiazolidinediones. *Diabetes Obes. Metab.* **7**(6), 675–691. https://doi.org/10.1111/j.1463-1326.2005.00497.x (2005).
73. Liu, J. et al. Combination of pioglitazone and metformin actions on liver lipid metabolism in obese mice. *Biomolecules*. **13**(8). https://doi.org/10.3390/biom13081199 (2023).
74. He, Z. et al. The roles and mechanisms of LncRNAs in liver fibrosis. *Int. J. Mol. Sci.* **21**(4). https://doi.org/10.3390/ijms21041482 (2020).
75. Chen, T. et al. The genome sequence archive family: toward explosive data growth and diverse data types. *Genom. Proteom. Bioinform.*, **19**(4), 578–583. https://doi.org/10.1016/j.gpb.2021.08.001. (2021).
76. Database Resources of the National Genomics Data Center. China National Center for bioinformation in 2022. *Nucleic Acids Res.* **50**, D27–D38. https://doi.org/10.1093/nar/gkab951 (2022).

Author contributions

YD Sun, JJ Han and CX Zhou conceptualised and designed the study. YD Sun, CX Wu and XL Gong were involved in collection, preparation, interpretation, validation and critical review of the data. YD Sun and XL Gong performed animal experiments. YD Sun, CX Wu and YM Li performed formal analysis including bioinformatics and statistical analyses. YD Sun and RQ Han drew the figures, designed and edited drafts of the manuscript and finalized the manuscript for submission. H Zhang and YM Li reviewed the literature and edited drafts of the manuscript. JJ Han reviewed the literature, prepared the table and prepared drafts of the manuscript. All authors contributed to the article and approved the submitted version.

Funding

This item was supported by the National Natural Science Foundation of China (NSFC No. 82272101) (JJ Han), and the National Key Research and Development Program of China (No.2018YFE0126500) (JJ Han), the Natural Science Foundation of Shandong Province (No. ZR2021MH060). The funding bodies played no role in the design of the study and collection, analysis, and interpretation of data and in writing the manuscript.

Declarations

Declaration of generative AI and AI-assisted technologies

This is to declare that all results and analyses presented in our paper were conducted solely by the authors, without the intervention of Artificial Intelligence (AI) or related technologies. We affirm that the data processing, interpretation, and conclusions drawn in this study were executed manually by the research team, ensuring that the insights and findings reflect our understanding and expertise in the subject matter. We did not employ AI tools or algorithms for data analysis or result generation, thus maintaining the integrity and authenticity of the research. During the preparation of this work the authors used ChatGPT 4.0 in order to improve language and readability. The authors reviewed and edited the content and took full responsibility for the content of the publication.

Competing interests

The authors declare no competing interests.

Additional information

Supplementary Information The online version contains supplementary material available at https://doi.org/10.1038/s41598-025-07557-7.

Correspondence and requests for materials should be addressed to Y.-d.S. or J.-j.H.

Reprints and permissions information is available at www.nature.com/reprints.

Publisher's note Springer Nature remains neutral with regard to jurisdictional claims in published maps and institutional affiliations.